Detection and Position Location of Partial Discharges in Transformers Using Fiber Optic Sensors

by

Lijun Song

Thesis submitted to the faculty of
the Virginia Polytechnic Institute and State University
in partial fulfillment of the requirements for the degree of

Master of Science
in
Electrical Engineering

Approved By:

Dr. Anbo Wang, Committee Chair

Dr. Yilu Liu, Committee Member

Dr. Kristie Cooper, Committee Member

December 3, 2004
Blacksburg, Virginia
U.S.A.

Keywords: Partial Discharge (PD), High Voltage Transformer (HVT), Fiber Optic Acoustic Sensor, Time Difference of Arrival (TDOA), Positioning Localization, Signal Processing

Detection and Position Location of Partial Discharges in Transformers Using Fiber Optic Sensors

Lijun Song

Abstract

Power transformers are one of the most important components in the electrical energy network. Extending transformer life is very economically valuable due to power outage. Therefore the development of instruments to monitor the transformer condition is of great interest. Detection of partial discharges (PDs) in power transformers is an effective diagnostic because it may reveal and quantify an important aging factor and provide information on the condition of the transformer. However, partial discharge diagnostics are still not effectively used for online monitoring of transformers because of the complexity of PD measurements and difficulties of discriminating of PDs and other noise sources.

This thesis presents a further study of detection and location of partial discharges in power transformers based on previous work conducted at the Center for Photonics Technology (CPT) at Virginia Tech. The detection and positioning system consists of multiple extrinsic Fabry-Parot interferometric (EFPI) fiber acoustic sensors which can survive the harsh environment of oil-filled transformers.

This thesis work is focused on optimal arrangement of multiple sensors to monitor and locate PD activities in a power transformer. This includes the following aspects. First, the sensor design requirements are discussed in order to successfully detect and accurately position the PD sources. In the following sections, Finite Element Method (FEM) is used to model the EFPI sensor fabricated at CPT. Experiments were conducted to measure the angular dependence of the frequency response of the sensor. It is shown that within the range of ±45º incident angles, the sensitivity varies by 3-5dB. Finally, the thesis demonstrates a PD positioning experiment in a 500 gallon water tank (R × H = 74'' × 30'' cylinder) using a hyperbolic positioning algorithm and time difference of arrival (TDOA). Finally we demonstrated that 100% of the positioning data is bounded by a $22.7 \times 4.1 \times 5.3\ mm^3$ cube, with a sensing range of 810 mm using the leading edge method with FIR filtering.

Acknowledgements

I would like to especially thank my advisor, Dr. Anbo Wang, for the guidance and support he has provided throughout the course of this work. His knowledge, guidance, energy, openness, and inspiration will always serve to me as an example of the professor.

Special thanks to Dr. Kristie Cooper for her guidance, advice, encouragement and criticism, and without whom, this thesis would not have been possible. Special thanks to Dr. Yilu Liu, the thesis committee, for her advice, comment and encouragement.

My appreciation goes to the members of the CPT staff. To Ms. Debbie Collins and Bill Cockey, thank you for all of the administrative support. Thank you to the students of the CPT for your help and support, especially Bing Yu for the help on the experiments, DaeWoong Kim for the help on sensor fabrications, Bo Dong for the help of making pictures, Zhuang Wang for the generous help on my experiments.

I would also like to thank my friends who kept me sane during my Master studies. To my friends, Jinye Zhang, Yuan Li, Xiaoying Li, Yong Wang, John Hoffer, Bing Liu, and Yi Zheng, thank you for the love and support you have given so freely over the past years. Finally, I want to mention those who do not need to be mentioned, because they are the very reason for my existence, my parents, brother, sisters and nephews, for their endless concern, love and support.

Table of Contents

Chapter1: Overview ---1

1.1 Partial discharges and insulation deterioration ------------------------------------1

1.2 Optical PD detection methods---2

1.3 PD location methods --3

1.4 Contribution to the field---4

1.5 Scope of the thesis work--5

References--6

Chapter2: Sensor Design and Principle of Operation------------------------------------8

2.1 Requirements for sensor design---8

2.1.1 Passband of the sensor---8

2.1.2 Sensitivity--8

2.1.3 Directionality---8

2.1.4 Sensor array layout---9

2.1.5 Multipath interference---9

2.2 EFPI sensor design---10

2.2.1 Sensor structure and principle--10

2.2.2 Sensor sensitivity--11

2.2.3 Natural frequency---13

2.3 Summary--14

References--14

Chapter3: Angular Dependence of the Frequency Response of EFPI Fiber Acoustic Sensor---16

3.1 Basic idea of ANSYS for coupled structural acoustic analysis-----------------17

3.2 ANSYS model for EFPI sensor--18

3.2.1 Two dimenional ANSYS model---19

3.2.2 Three dimensional ANSYS model--------------------------------------22

3.2.3 Comparison of the ANSYS results with theory------------------------28

3.3 Experiments measuring the angular dependence of the frequency response--29

3.3.1 *Basic idea*--29

3.3.2 *Experimental setup*---30

3.3.3 *Experimental Results*--32

3.4 Conclusion--36

References---37

Chapter 4: Position Location of Partial Discharge---38

4.1 Positioning algorithm--39

4.2 PD location using different methods---40

4.2.1 Experimental setup--40

4.2.2 Effects of AWGN noise and multi-channel interference-------------41

4.2.3 PD location using convolution method------------------------------- 43

4.2.4 PD location using cross correlation method--------------------------44

4.2.5 PD location using leading edge method with digital FIR filter-----46

4.2.6 Relationship between positioning accuracy and sensor array layout--49

4.3 Evaluation of the experimental results---49

4.3.1 Cross-correlation method--51

4.3.2 Leading edge method with FIR filter---------------------------------54

4.3.3 Convolution method--57

4.3.4 Discussion--60

References---62

Chapter 5: Summary and future work---63

5.1 Summary of the work--63

5.2 Future work---64

Appendix 1: Program for angular frequency response in Ansys 7.0-----------------------66

Appendix 2: Matlab script for position location--71

List of Figures

Figure 2.1, Schematic diaphragm of layout of sensor array in transformer tank-----------9
Figure 2.2, Schematic diagram of sensing system---11
Figure 2.3 Schematic diagram of EFPI sensor--11
Figure 2.4, Schematic diagram of sensor head ---12
Figure 3.1, Schematic diagram of the relationship between the acoustic wave direction and the sensor ---19
Figure3.2, Meshed model of the sensor in the fluid--20
Figure 3.3, Frequency response of the diaphragm in water---------------------------------21
Figure 3.4, Pure mechanical frequency response of the diaphragm------------------------21
Figure 3.5, Meshed sensor diaphragm (upper surface) and supporting tube---------------22
Figure 3.6, The lowest order mode shape of the diaphragm---------------------------------23
Figure 3.7, Contour plot of the deflection of the diaphragm--------------------------------24
Figure 3.8, Results of harmonic analysis--24
Figure 3.9, Three dimensional ANSYS model in fluid--------------------------------------25
Figure 3.10 Frequency reponse from harmonic analysis------------------------------------26
Figure 3.11, Angular dependence of frequency response of the sensor -------------------27
Figure 3.12, Angular dependence the sensor for frequencies at 160 kHz and 180 kHz---27
Figure 3.13, Directivity patterns for a piston in a rigid baffle, a piston in a soft baffle and an unbaffled piston. ---29
Figure 3.14, Block diagram of the basic idea of transfer function measurements--------30
Figure 3.15, Schematic diagram of experimental setup-------------------------------------31
Figure 3.16, Connections of experimental setup for angular dependence of the frequency response ---31
Figure 3.17, Realistic experiment outlook inside tank-------------------------------------32
Figure 3.18, Received signal from sensor with multi-path interference-------------------33
Figure 3.19, Sensor frequency response for 0 degree incidence---------------------------33
Figure 3.20, Angular dependence of the frequency response------------------------------34

Figure 3.21, Angular dependence of the frequency response of the sensor at 160 kHz and 180 kHz--35
Figure 4.1, Coordinate system with four sensors and one acoustic source---------------40
Figure 4.2, Detected acoustic waveforms for each sensor----------------------------------41
Figure 4.3, Two different samples of the detected acoustic waveforms from sensor 1--42
Figure 4.4, Multi-path interference signals--42
Figure 4.5, Convolution of the waveforms between sensor k (k = 1,2,3,4) and sensor 1---43
Figure 4.6, Positioning results using convolution method----------------------------------44
Figure 4.7, Cross-correlation the waveforms between sensor k (k = 1,2,3,4) and sensor 1---45
Figure 4.8, Positioning results using cross correlation method------------------------------46
Figure 4.9, Frequency response of the FIR filter (green trace: phase response, blue trace: magnitude response)--47
Figure 4.10, Two representative waveforms form sensor 1 after FIR filter ----------------48
Figure 4.11, Positioning results using leading edge method with FIR filter (red) and without filter (green)--48
Figure 4.12, Positioning results using cross-correlation method ---------------------------52
Figure 4.13, The position data (red square) within the ±50 mm cube----------------------52
Figure 4.14, Histogram of the positioned data in x (a), y (b) and z (c) axes using the cross-correlation method---54
Figure 4.15, Position location results (red star) using FIR filter method-------------------55
Figure 4.16, Positioning results (red square) within the ±50 mm cube---------------------55
Figure 4.17, Histogram of the positioning data in x (a), y (b) and z (c) axes using the leading edge method with FIR filter---57
Figure 4.18, Positioning result using convolution method -------------------------------58
Figure 4.19, Distributions of the positioning results within the ±50 mm error cube------58
Figure 4.20, Histogram of the positioning data in x (a), y (b) and z (c) axes using the convolution method--60

List of Tables

Table 2.1, Properties of material in use--12

Table 4.1, Comparison of positioning results using different methods with the source located at (8.4, 446.1, 409.3). (The units are all in millimeters)----------------------------49

Table 4.2, Coordinate system for the sensor and the PD source-----------------------------51

Chapter 1 Overview

Power transformers represent the largest portion of capital investment in transmission and distribution substations. The financial consequence of losing a single unit can have a multimillion-dollar impact. Thus, monitoring the running condition of power transformers and taking action before catastrophic failures is very important to prevent power systems from outages and secondary losses. Normally, faults in power transformers are caused by the decreasing of dielectric strength and dielectric breakdown during service life due to the cumulative effect of the thermal, electrical and mechanical stresses [1]. Dielectric breakdown in transformers is most frequently initiated by partial discharges (PDs) [2]. It is therefore important to monitor and locate the partial discharge activities in a transformer on line on an early stage to anticipate the possibility of insulation problem, and further, to prevent catastrophic failure [3].

1.1 Partial discharges and insulation deterioration

A partial discharge can be described as an electrical pulse or discharge in a gas-filled void or on a dielectric surface of a solid or liquid insulation system [4]. This pulse or discharge only partially bridges the gap between phase insulation to ground, or phase-to-phase insulation. A full discharge would be a complete fault between line potential and ground. These discharges might occur in any void between the conductor and the ground. The voids may be located between the conductor and insulation wall, or internal to the insulation itself, or between the outer insulation wall and the ground frame. The pulses occur at high frequencies; therefore, they attenuate quickly as they pass through a short distance. The discharges are effectively small sparks occurring within the insulation system, therefore deteriorating the insulation, and can eventually result in complete insulation failure.

Partial discharge in power transformers may occur due to various causes including over voltage, over heating, chemical or mechanical deterioration of the materials, particles in the oil, static electrification, a defect in the insulation, a loose connection, floating objects arcing under the oil, etc. Depending on the cause involved, a discharge may occur in a pre-existing gas phase (bubbles, cavities), or in the oil itself (in the liquid bulk or at the oil/pressboard interface) [5]. Since serious partial discharges may reflect the possibility of system breakdown, and consequently power network failure, it is important to monitor and locate partial discharges.

1.2 Optical PD detection methods

Partial discharges generate both physical phenomena (including electrical, acoustic and optical phenomenon) and chemical changes. Consequently PD detection can be generally categorized into electrical, acoustic, optical and chemical methods [6, 7, 8]. Electrical and acoustic methods are both widely applied for PD monitoring in oil filled transformers. Further details about the principles and comparisons of these methods can be found in references 6, 7 and 8. This section will mainly focus on recent progress in optical methods for PD detection. Currently, fiber optic sensors are considered one of the best options for monitoring high voltage equipment, such as power transformers and generators, due to their chemical and electrical inertness and capability of surviving the harsh environment of the interior of high voltage equipment without compromising or altering the functionality of the device.

One early experiment was conducted to detect partial discharges in the air and SF_6 using fluorescent fibers [9]. The fluor which is dissolved in the fiber core can be illuminated by light whose wavelength falls within the absorption spectrum of the fluor. The fluor absorbs photons and reemits isotropically in the fiber core. However, this PD monitoring method does not attract too much attention for two reasons. One is that in reality, the strength of light generated by partial discharge is not very strong in the electromagnetic environment with SF_6 as the ambient atmosphere. The second reason is that the reemitted light is not a guided mode in fiber. Therefore, the strength of light at the receiver side is normally too weak to be detected.

Another optical method is to use a fiber coil [10] as the sensing element. Actually, this method combines both optical and acoustic methods. Detection is based on the photoelastic effect of the silica fibers. The acoustic wave that impinges on the optical fibers will cause deformation of the optical fiber structure. This deformation in turn will change the fiber refractive index and fiber length. The light wave is therefore phase modulated by the acoustic wave, and this change can be extracted by a homodyne demodulator. Because the silica fiber has relatively low photoelastic effect, a long length of fiber is needed to increase the sensitivity. However, the longer the fiber, the bulkier the coil, and the greater temperature dependence of the sensor. Also, bending loss limits the minimum diameter the fiber coil can reach. The bulky size of this sensor made its sensitivity more angular dependent.

A third type of fiber based sensor for PD detection is the extrinsic Fabry-Perot interferometer (EFPI) [7, 8]. The diaphragm, the sensing element of this kind of sensor, deflects as the acoustic pressure interacts with it. This deflection will cause a phase lag in one optical path of the FP interferometer, thus affecting the interference pattern of the optical signal. Partial discharge is detected by the change in the interference pattern. This type of sensor is the subject of this thesis. Detailed principles of operation will be given in the following chapters. Because this type of sensor uses a diaphragm as the sensing element, the size of the sensor head can be made very small (diameter below 2 millimeters). Considering the velocity of the acoustic sound in transformer oil is about 1400 m/s, the wavelength for the frequency range of 100 kHz to 300 kHz is from 14 mm to just under 5 mm. So this EFPI sensor will be less angular dependent compared with the fiber coil sensor.

1.3 PD Location methods

Location of a PD source is another important issue for transformer diagnostics. Usually it is fulfilled by multiple triangulation methods using several piezoelectric microphones placed around the outside of the transformer tank [7, 8]. This method suffers greatly from the attenuation of the acoustic signal by the tank wall, and the multipath crosstalk caused by the different transmission speed of the acoustic wave in the solid and liquid insulations and the tank wall.

There are two known techniques for electrical PD measurements [11]: narrow band and wide band. The narrow-band method is usually used for offline measurements, in which the apparent charge can be detected, but localization, indispensable for good maintenance, cannot usually be performed. The wide-band method, in contrast, offers both a determination of the apparent charge and PD position. The apparent charge of the PD can be evaluated similarly to narrow-band measurements. PD localization can be made by analyzing the shape of the PD signal. PDs are distorted on their way from their points of origin to the detection point. The amount of distortion will depend upon several factors, including the distance from the discharge source and the detection impedance. Through analyzing the terminal signals caused by PDs and extracting the spectra features related to different locations, a feature template matching algorithm can be developed for locating the PD sources [12]. The experiments indicated that a location accuracy of better than 5% of the winding length can be normally achieved. Another example exploits the transfer function of the transformer coils to evaluate and localize PDs [11]. A major difficulty with electrical methods is the suppression of noise and external disturbances that are similar to the PD signal and affect the accuracy and sensitivity of detection. Furthermore, because of the complicated structure of a transformer winding, it is still difficult to take the distortion into account.

The fiber acoustic sensor has the advantage of being chemically inert and electrically non-conducting, thus can be placed inside of the transformer tank. This intrusive detection greatly reduces the multipath interference compared with piezoelectric acoustic sensor. The fiber acoustic sensor is also immune to electromagnetic interference. If designed properly, a fiber acoustic sensor can receive much cleaner PD signals and a relatively high signal to noise ratio, which are important to improve the PD location accuracy. When multiple sensors are placed inside of the transformer tank, triangulation can be performed to locate the PD sources by determining the relative time delays. This will be the subject of Chapter 4 in this thesis.

1.4 Contributions to the field

This thesis work contributes to the field of PD detection and localization in the following aspects.

1. Sensor parameters which are critical for successfully detecting PD activities were discussed. An optimal sensor array layout was investigated based on the sensing scope, angular dependence of frequency response and successful PD localization.

2. An ANSYS model to analyze the angular dependence of frequency response was built. Angular dependence of the frequency response of the sensor was experimentally tested. The test results gave the frequency response of the ±45 degree

range incident angle to the sensor. This angular dependence of the frequency response can help to design the sensor array layout.

3. Partial discharge detection and localization are realized using hyperbolic position fixing solution based on the time difference of arrival (TDOA). Compared to the previous work at CPT [7], two new signal processing methods, cross-correlation and the leading edge method using a digital FIR filter, are used to find time delays. Experimental results show that better localization results can be achieved using cross-correlation method and leading edge method with digital FIR filter than using convolution method.

1.5 Scope of the thesis work

Much work has been done on the detection and location of partial discharges. This thesis presents the latest results of partial discharge detection and location using EFPI fiber acoustic sensors developed CPT.

Chapter 1 is the overview of the background of the project, including partial discharges and the progress of PD discharge detection and location methods.

Chapter 2 presents the sensor design requirements for PD detection in oil filled power transformers. These requirements include the frequency range, sensitivity, directionality, sensor array layout, and noise effects. Based on these requirements, a design of an EFPI sensor is discussed and the principle of operation is briefly described.

Chapter 3 focuses on the frequency response of the EFPI sensor. A two dimensional and three dimensional simulation model of the EFPI sensor are developed using Finite Element Methods (FEM) in Ansys 7.0 environment. An experiment is carried out to test the sensor’s directionality.

Chapter 4 investigates the hyperbolic positioning of partial discharge sources using time difference of arrival (TDOA). The effect of additive white Gaussian noise and multipath interference on the accuracy of positioning is discussed. The convolution method, cross-correlation method and leading edge method with digital FIR filter are used to fight the noise and improve the positioning accuracy. An evaluation of the positioning results is given at the end of the Chapter 4.

Chapter 5 summarizes the entire thesis work and suggests the future work.

Reference:

1. Abbas Zargari, Trevor R. Blackburn, “Application of optical fiber sensor for partial discharge detection in high-voltage power equipment”, 1996 IEEE annual report, Conference on Electrical Insulation and Dielectric Phenomena, San Francisco, pp. 541-544, Oct, 1996.
2. S. N. Hettiwatte, Z.D. Wang, P.A, Crossley, P.Jarman, G.Edwards and ADarwin, et, al, “An electrical PD location method applied to a continuous disc type transformer winding”, Proceedings of the 7th International Conference on Properties and Applications of Dielectric Materials, June 1-5, 2003, Nagoya, P2-43, pp. 471-474.
3. Andreas Kelen, “Trends in PD diagnostics when new options proliferate, so do old and new problems”, IEEE Transactions on Dielectrics and Electrical Insulation, vol. 2(4), pp. 529-534, 1995.
4. Gabriel J. Paoletti and Alexander Golubev, “Partial Discharge Theory and Technologies Related to Medium-Voltage Electrical Equipment”, IEEE Transaction on Industry Applications, vol. 37, no. 1, pp, 90-103, 2001.
5. H. Debruyne and O. Lesaint, “About the significance of PD Measurements in Liquids”, IEEE Transactions on Dielectrics and Electrical Insulation, vol. 10 (3), 2003.
6. I. J. Kemp, "Partial discharge plant-monitoring technology: Present and future developments," IEE Proc.-Sci. Meas. Technology, vol. 142, pp. 4-10, 1995.
7. Alison K. Lazarevich, “Partial Discharge Detection and Localization in High Voltage Transformers Using an Optical Acoustic Sensor”, Virginia Tech Masters Thesis, May 2003.
8. Jiangdong Deng, Hai Xiao, Wei Huo, Ming Luo, Russ May, Anbo Wang, and Yilu Liu, "Optical fiber sensor-based detection of partial discharges in power transformers," Optics and Laser Technology, vol. 33, pp. 305-311, 2001.
9. R. Mangeret, J. Farenc, Vui Ai, P. Destruel, D. Puertolas, “Optical detection of partial discharges using fluorescent fiber”, IEEE Transactions on Electrical Insulation, vol. 28, no. 4, pp. 783-789, 1991 .

10. Zhao Zhiqiang, Mark MacAlpine, and M. Süleyman Demokan, “The Directionality of an Optical Fiber High-Frequency Acoustic Sensor for Partial Discharge Detection and Location”, Journal of Lightwave Technology, vol. 18, no. 6, pp. 795-806 , 2000.
11. Akbari A, Werle P, Borsi H, Gockenbach E. “Transfer function-based partial discharge localization in power transformers: a feasibility study”. IEEE Electrical Insulation Magazine, vol.18, no.5, pp.22-32, Sept.-Oct. 2002.
12. Z. D. Wang, P. A. Crossley, K. J. Cornick and D. H. Zhu, “An algorithm for partial discharge location in distribution power transformers”, 2000 IEEE Power Engineering Society Winter Meeting. Conference Proceedings (Cat. No.00CH37077), Piscataway, NJ, USA, vol.3, pp.2217-22, 2000.

Chapter 2 Sensor Design and Principle of Operation

The nature of partial discharge determines the design of the sensor. A thorough investigation of the nature of partial discharge is necessary, but not the subject of this thesis. In this chapter, the requirements for the sensor design are summarized based on the previous research works on partial discharges. Then the structure and principle of an extrinsic Fabry-Perot interferometer (EFPI) sensor for this project follows.

2.1 Requirements for sensor design

2.1.1 Passband of the sensor

Ideally, the sensor should be able to respond to the entire bandwidth of partial discharges and reject as much noise bandwidth as possible. The frequency range of the partial discharges can reach 300 kHz, but tends to concentrate within 100 kHz to 200 kHz [1, 2, 3, 4, 6]. However, there is a noise bandwidth centered at 50 ~ 60 kHz due to the effect of core noise, oil circulation disturbance and other environmental noise [2, 5, 6]. So the sensor bandwidth should be designed between 100 kHz to 300 kHz.

2.1.2 Sensitivity

The rms sound pressure at 100 millimeter from a 1-pC discharge is 0.2 Pa and a meter away will be 0.02 Pa [2]. The discharges in a practical power transformer are of tens to thousands of pico–coulombs. Therefore, the sensor should be able to detect pressure of 0.2 Pa with a considerably good signal to noise ratio [2, 7]. On the other hand, the sensor should not distort waveforms of the partial discharges when a PD gets very strong. Undistorted waveforms can be used for successful location of the PD site. If distortion is introduced, considerable positioning error will be inevitable and if worse, will fail to locate PDs. Therefore, the sensor should have a linear response from 0.2Pa to 10000 Pa.

2.1.3 Directionality

Partial discharge can happen anywhere inside a transformer. After the sensor is installed inside the transformer tank, it should be able to respond to any single partial discharge without any adjustment. When the sensor is directly facing the partial discharge, it will produce the maximum response. However, when the sensor is facing away from the PD source, the sensor may fail to detect partial discharge activity. We hope that the sensor can ‘see’ as much space as possible. So the angular dependence of the frequency response has to be determined and taken into account in system design.

2.1.4 Sensor array layout

As mentioned before, in order to locate a partial discharge by triangulation, the sensor should be able to see as large a space as possible. Considering a rectangular transformer tank with coils (Figure 2.1), the best configuration is to set one sensor at each corner of the tank, facing away from the corner. In this configuration, each sensor has a view of the internal transformer with a maximum angle of 45 degrees. However, more sensors are needed to monitor the partial discharges between the coils.

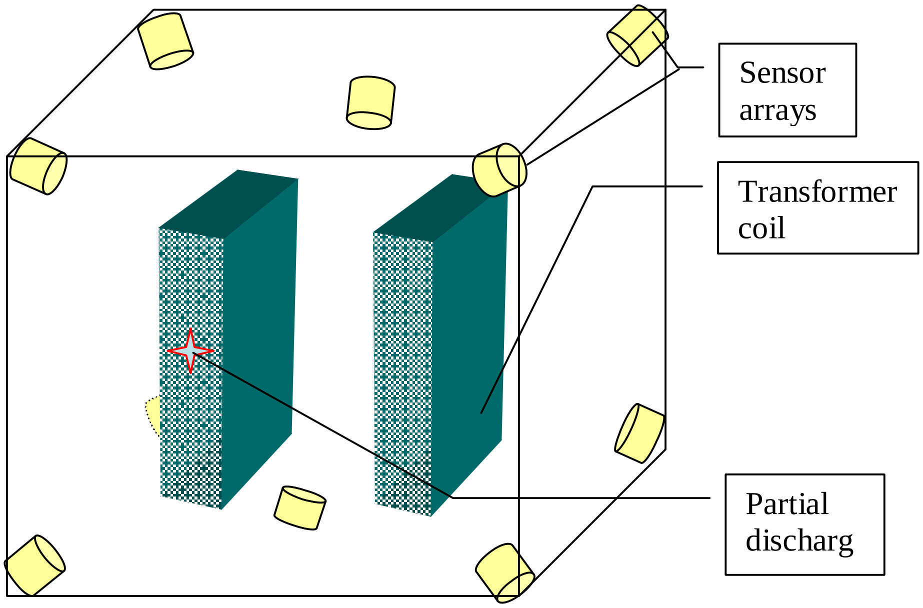

Figure 2.1, Diaphragm of sensor array layout in transformer tank.

2.1.5 Multipath interference

It is possible that there are multiple paths for the acoustic wave generated by a PD to travel to the same sensor even when we put the sensors inside the transformer. This multipath interference is mainly caused by the wall reflections instead of the different sound velocities between the oil and the wall of the transformer. If the distance between the multipath is really small, the detected PD signal will fluctuate in both amplitude and phase. If the time difference between the multipath is a little bit longer than the pulse width, the multipath signal will become noise that can not be averaged to zero. This will affect the signal to noise ratio and reduce the positioning accuracies. Therefore, measures have to be taken to either reduce multipath interference, or increase the difference of the multipath distances.

2.2 EFPI sensor design

2.2.1 Sensor structure and principle

The structure of the sensor in this project is an extrinsic Fabry-Perot interferometer (EFPI) sensor [8, 9]. Figure 2.2 is a diagram of the sensor system. 1300nm LED light is injected into the sensor head through a 3 dB coupler and a single mode fiber. The sensor head (Figure 2.3) consists of an EFPI cavity formed by a single mode optical fiber secured in a silica tube and a deformable silica diaphragm. The light will be partially reflected by the two surfaces in the sensor head, the fiber end and the diaphragm. The two reflected signals are recombined and transmit back to the 3dB coupler through the single mode fiber. At the other end of the coupler, a photodetector is connected to detect the signal. The interference pattern formed by the two reflected waves is processed in the signal processing unit.

An incident acoustic wave will deform the diaphragm and modulate the cavity length. This change in cavity length will result in a change of the interference pattern, thus a change in light intensity at the signal processing unit. [8, 9] give the relationship between the change in light intensity and the change in the cavity length. The linear range takes approximate 60% of one half interference fringe, the center of which is the static working point of the sensor. Therefore, the maximum deflection of the diaphragm should be within ±30% of a half fringe, almost ±200 nanometers.

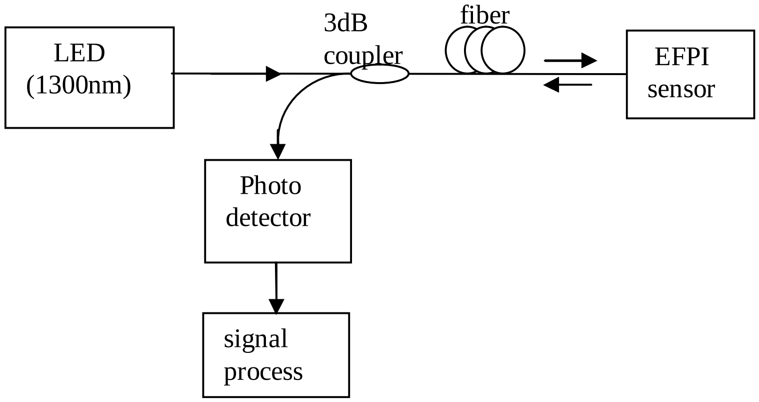

Figure 2.2 Diagram of sensing system

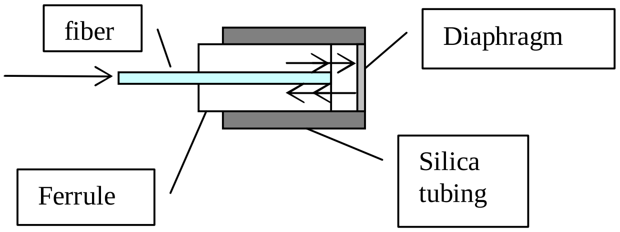

Figure 2.3 Diagram of EFPI sensor

2.2.2 Sensor sensitivity

Figure 2.4 is a schematic diagram of the sensor head. As mentioned before, the change in the interference pattern is caused by the pressure applied by acoustic waves. M. D. Giovanni gave the expression for the deflection of a round diaphragm with fixed edges loaded by lateral pressure P at any radial distance r as [10]

$$\frac{z}{P} = \frac{3(1-m^2)}{16Eh^3}(a^2 - r^2)^2 \qquad (2.1)$$

where z = defection

P = pressure

h = thickness of diaphragm

a = radius of diaphragm

E = modulus of elasticity

r = radial distance

m = Poisson’s ratio

The maximum deflection z_0 occurs at the center of the diaphragm where r = 0.

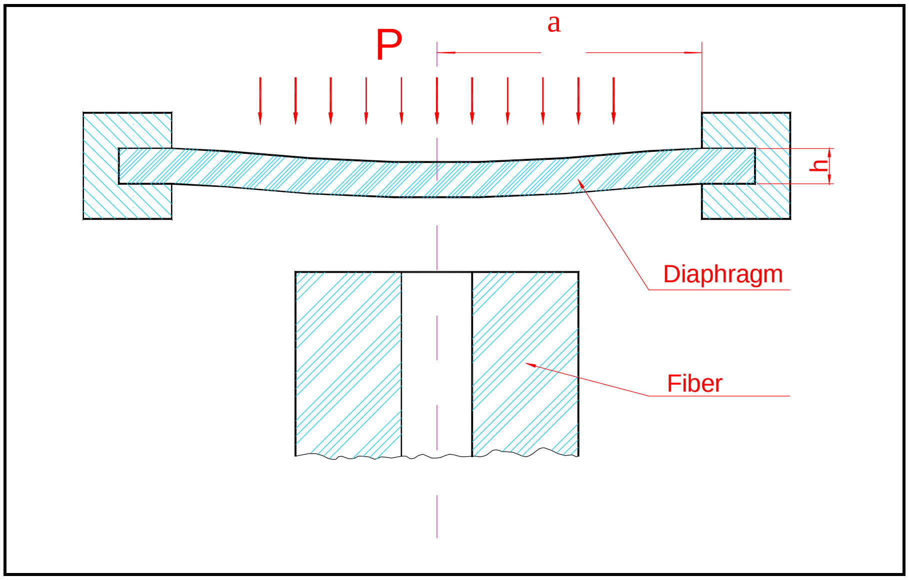

Figure 2.4, Schematic diagram of sensor head

Table 2.1, Properties of material in use

Material	Properties	Value
Fused Silica	Young's Modulus	73 GPa at 25°C
	Poisson's Ratio	0.17 at 25°C
	Density	2201 kg/m^3
	Dimension	Thickness: 0.15mm Diameter: 2.5mm
water	Density	1000 kg/m^3
	Sonic Velocity	1480 m/s

Using the parameters listed in Table 2.1, the sensitivity for the center of the sensor's diaphragm can be calculated to be 1.8×10^{-9} mm/Pa. The maximum deformation for a static pressure of 10000Pa will be 0.018 micron at the center of the diaphragm. However, when the applied acoustic wave is centered at the natural frequency of the diaphragm, the maximum deflection is much greater than this value.

2.2.3 Natural frequency

M. D. Giovanni gave the expression for the lowest natural frequency of a round diaphragm clamped at the edge as [10]

$$f_n = \frac{a\,h}{2p\,a^2}\sqrt{\frac{E}{12w(1-m^2)}} \tag{2.2}$$

where, α is a constant defined by the vibration mode. For the lowest order mode, α = 10.21. a, h, E and μ are as stated above, w is the specific weight of the material (density).

When the diaphragm is used to measure liquid pressure, the natural frequency is appreciably reduced due to the inertia of the liquid. If the diaphragm is used in a gas, there will not be any appreciable deterioration of frequency response. In fact, in a condition where a volume of gas is trapped behind the diaphragm, a slight increase in frequency is possible as the trapped gas might act as a stiffening spring.

If the diaphragm vibrates in a fluid, especially a liquid, the natural frequency maybe lowered considerably. The frequency equation (2.2) should be replaced by

$$f_2 = \frac{f_n}{\sqrt{1+b}} \tag{2.3}$$

where

$$b = 0.669\frac{w_1 a}{wh} \tag{2.4}$$

and w_1/w is the ratio of the densities of the fluid to the density of the material of the diaphragm.

Considering the parameters in Table 2.1, we can easily calculate the natural frequencies of the diaphragm as 263 kHz in air and 140 kHz in water. Because the real sensor has some air trapped inside of the sensing cavity, the actual value should be larger than 140 kHz. This sensor design places the natural frequency of the sensor at the center frequency of a typical partial discharge. It has the advantage of being able to detect weak partial discharge signals. One disadvantage is the frequency response is not flat over the PD frequency range of 100 kHz to 300 kHz.

The passband of the sensor system is further limited by the signal processing unit. In this system, a 300 kHz low pass filter is used in the signal processing unit. Thus noise from the sensor higher than 300 kHz is limited by the system.

2.3 Summary

In this chapter, several aspects of the sensor design for PD detection in transformers are considered. These include the sensor frequency range, sensitivity, directionality, sensor array layout and the multipath interference. The structure and the operation principle of an EFPI sensor designed for PD detection are described. The sensitivity and the frequency range of the sensor are calculated. However, the angular sensitivity, the sensor array layout and multipath effect are not discussed. They are the subjects of the next two chapters.

References:

1. T. Boczar, “Identification of a Specific Type of PD from Acoustic Emission Frequency Spectra, IEEE Transaction on Dielectrics Electrical Insulation”, vol. 8, no. 4, pp. 598- 606, 2001.
2. Mark MacAlpine, Zhao Zhiqiang, M. Suleyman Demokan, “Development of a fiber-optic sensor for partial discharges in oil-filled power transformers”, Electric Power System Research, vol. 63, pp. 27-36, 2002
3. P. M. Eleftherion, "Partial Discharge XXI: Acoustic Emission-Based PD Source Location in Transformers," in IEEE Electrical Insulation Magazine, vol. 11, pp. 22-26, 1995.
4. Zhao Zhiqiang and Yuan Yiquan, “Recent study of acoustic emission locating for partial discharge in UHV transformers and shunt reactors”, IEEE Trans. Electrical Insulation, vol. 3, no. 4. pp. 634- 638, 1988.
5. L. E. Lundgaard, “Partial discharge – Part XIV: Acoustic Partial Discharge Detection- Practical Application”, IEEE Electrical Insulation Magazine, vol. 8, no. 5, pp. 34- 43, 1992.
6. I. J. Kemp, "Partial discharge plant-monitoring technology: Present and future developments," IEE Proc.-Sci. Meas. Technology, vol. 142, pp. 4-10, 1995.

7. Zhao Zhiqiang, Mark MacAlpine, and M. Süleyman Demokan, “The Directionality of an Optical Fiber High-Frequency Acoustic Sensor for Partial Discharge Detection and Location”, Journal of Lightwave Technology, vol. 18, no. 6, pp. 795-806 , 2000.
8. Jiangdong Deng, Hai Xiao, Wei Huo, Ming Luo, Russ May, Anbo Wang, and Yilu Liu, "Optical fiber sensor-based detection of partial discharges in power transformers," Optics and Laser Technology, vol. 33, pp. 305-311, 2001.
9. Alison K. Lazarevich, “Partial Discharge Detection and Localization in High Voltage Transformers Using an Optical Acoustic Sensor”, Virginia Tech Masters Thesis, May 2003.
10. Giovanni, Flat and corrugated diaphragm design handbook, vol. 11. New York: M. Dekker, 1982.

Chapter 3 Angular Dependence of the Frequency Response of the EFPI Fiber Acoustic Sensor

The deflection of the diaphragm in response to an acoustic wave is dependent on the angle at which the acoustic wave is incident [1]. This angular dependence defines the spatial range that the sensor can detect. Therefore this information is very helpful in determining how many sensors will be needed and what the configuration of the sensor array should be in order to successfully monitor the PD activities all over the transformer tank. Practical measurements [2] and semi-analytical efforts [3] have been made previously to analyze the angular dependence of the frequency response of the sensor. However, the angular dependent response depends on a number of factors that are difficult to qualify. The size and shape of the sensing head are the most important factors determining the angular dependent response. The sensor design, material used and the assembly method can also play an important role and affect the angular dependence of the frequency response. In general, there is no such universal way to give the angular dependent response of the sensor. An alternate way of analyzing the interaction of the incident acoustic wave and the sensing head is using finite element methods (FEM) [4]. Finite element methods have the advantage of analyzing an individual case in which one can use information specific to the sensor to gain more accurate results.

In this section, an ANSYS FEM model is built to investigate the angular dependence of the frequency response of the PD sensor described in the sensor design section. First, an introduction of ANSYS for finite element methods is given. Then both two and three dimensional FEM models are built in ANSYS 7.0 and the angular dependence of the frequency response of the sensor is given. Next, an experiment to measure the angular dependence of the frequency response is demonstrated. The experimental results are compared with those of the ANSYS model. Finally, the sensor array layout and the number of sensors needed in the system are discussed based on the obtained results.

3.1 Basic idea of the ANSYS for coupled structural acoustic analysis

The acoustic analysis in the ANSYS/Multiphysics and ANSYS/ Mechanical programs only involves modeling the fluid medium and the surrounding structure [5]. Typical quantities of interest are the pressure distribution in the fluid at different frequencies, pressure gradient, particle velocity, the sound pressure level, as well as scattering, diffraction, transmission, radiation, attenuation, and dispersion of acoustic waves. A coupled acoustic analysis takes the fluid-structure interaction into account. The acoustic pressure in the fluid medium is determined by the wave equation with the following assumptions:

1. The fluid is compressible (density changes due to pressure variations).
2. The fluid is inviscid (no dissipative effect due to viscosity).
3. There is no mean flow of the fluid. The mean density and pressure are uniform throughout the fluid. Note that the acoustic pressure is the excess pressure above the mean pressure.
4. Analyses are limited to relatively small acoustic pressures so that the changes in density are small compared with the mean density.

The interaction of the fluid and the structure at a mesh interface causes the acoustic pressure to exert a force applied to the structure and the structural motions produce an effective "fluid load." The governing finite element matrix equations then become:

$$[Ms]\,\{\ddot{U}\} + [Ks]\,\{U\} = \{Fs\} + [R]\,\{P\} \tag{3.1}$$

$$[M_f]\,\{\ddot{P}\} + [K_f]\,\{P\} = \{F_f\} - \rho_0\,[R]^T\,\{\ddot{U}\} \tag{3.2}$$

[R] is a "coupling" matrix that represents the effective surface area associated with each node on the fluid-structure interface (FSI). {P} and {U} are the fluid pressure and the structure displacement, respectively. $[M_f]$ is the fluid mass matrix, $[K_f]$ is the fluid stiffness matrix, and ρ_0 is the fluid density. $\{F_f\}$ is the applied fluid pressure load vector at the interface obtained by integrating the pressure over the area of the surface. Correspondingly, [Ms] is the structure mass matrix, [Ks] is the structure stiffness matrix, and, $\{F_f\}$ is the applied structure pressure load vector at the interface .The coupling matrix [R] also takes into account the direction of the normal vector defined for each pair of coincident fluid and structural element faces that comprise the interface surface. The positive direction of the normal vector, as the ANSYS program uses it, is defined to be outward from the fluid mesh and in towards the structure. Both the structural and fluid load quantities that are produced at the fluid-structure interface are functions of unknown nodal degrees of freedom. Placing these unknown "load" quantities on the left hand side of the equations and combining the two equations into a single equation produces the following:

$$\begin{bmatrix} M_s & 0 \\ \rho_0 R^T & M_f \end{bmatrix} \begin{pmatrix} \ddot{U} \\ \ddot{P} \end{pmatrix} + \begin{bmatrix} K_s & -R \\ 0 & K_f \end{bmatrix} \begin{pmatrix} U \\ P \end{pmatrix} = \begin{pmatrix} F_s \\ F_f \end{pmatrix} \qquad (3.3)$$

Equation 3.3 implies that nodes on a fluid-structure interface have both displacement and pressure degrees of freedom.

We can solve the acoustics problem by performing a harmonic analysis. The analysis calculates the pressure distribution in the fluid due to a harmonic (sinusoidally varying) load at the fluid-structure interface. By specifying a frequency range for the load, we can observe the pressure distribution at various frequencies. Peak harmonic response occurs at forcing frequencies that match the natural frequencies of the structure. Before obtaining the harmonic solution, we should first determine the natural frequencies of the structure by obtaining a modal solution.

A three dimensional ANSYS model is described in this section. First, the pure mechanical frequency response of the sensor and the frequency response for the sensor immersed in water are simulated and the results are compared with the analytical results. Then the model for angular response in water is given and the results are compared with that of the analysis.

3.2 ANSYS model for EFPI sensor

In order to get the frequency response of the PD sensor, the sensor head and the surrounding fluid are modeled in ANSYS by finite element methods. Figure 3.1 is a diagram of a sensor head immersed in the fluid. When the propagation direction of the acoustic wave is perpendicular to the surface of the diaphragm (red arrows in Figure 3.1), the model is cylindrically symmetric and a simple two dimensional ANSYS model can be exploited. However, when the angle between the propagation of the acoustic wave and the surface direction of the diaphragm is not 0, the model is no longer axially symmetric and a three dimensional model has to be built.

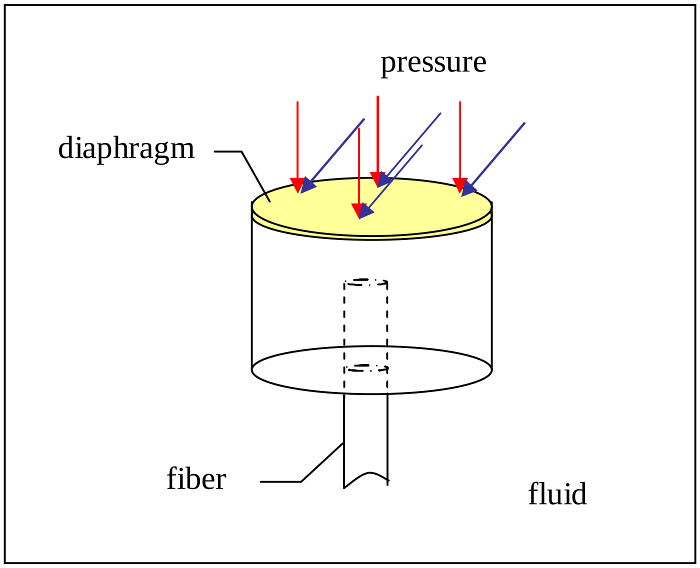

Figure 3.1, Schematic diagram of the relationship between the acoustic wave direction and the sensor.

3.2.1 Two dimensional model

We first consider that the acoustic pressure is perpendicular to the diaphragm. Taking advantage of the axial symmetry, we can build a two-dimensional finite element model. The model consists of a piece of diaphragm, a supporting tube and a fluid region whose boundary is 0.2 times the wavelength away from the structure. The supporting cylindrical tube also functions to isolate fluid from the internal part of the sensor. The fluid (water) is modeled with 2D acoustic elements (fluid29) and the silica diaphragm is modeled by 2D solid elements (solid42). The meshed two-dimensional model is shown in Figure 3.2. Because this model is used to analyze the deformation of the diaphragm when the acoustic wave is applied, we don't include the fiber pigtail in the model for simplification. This simplification will not affect the analysis results. The fluid structure interface is set between the fluid and the structure. An absorption layer is formed along the outer edge of the fluid body to set the fluid boundary condition. The degrees of freedom (DOFs) for the nodes along the diaphragm's edge and for all the supporting tubing are set to 0 as part of the boundary conditions. We make the assumption that the deformation of silica diaphragm is linear (thickness of diaphragm is 125 microns; maximum deflection is less than 10 microns, < 20% deflection).

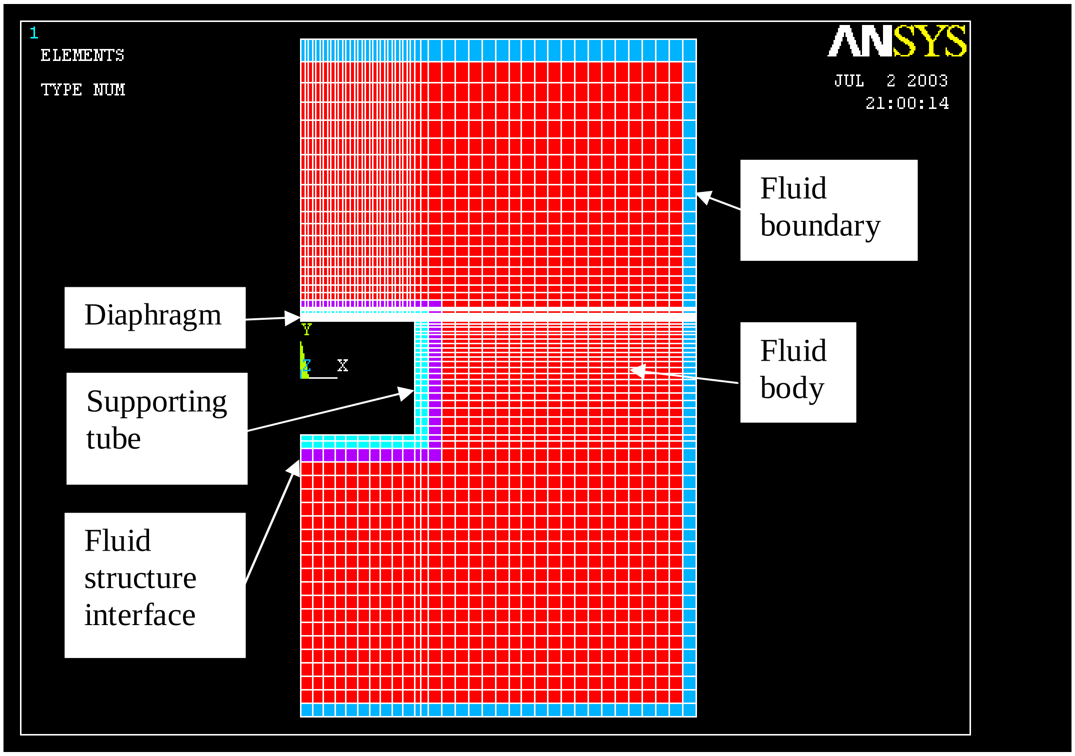

Figure3.2, Meshed model of the sensor in the fluid.

The diaphragm material is fused silica, with a Young’s modulus of 7.3e10 Pa, density of 2201 kg/m^3, and Poisson’s ratio of 0.17. The diaphragm is a thin round plate with a diameter of 2.5mm and thickness of 125 microns. The fluid is composed of water with a density of 1000 kg/m^3 and a sonic velocity of 1480 m/s.

The result of the harmonic analysis (Figure 3.3) shows the natural frequency is 148 kHz, which matches the analytical result (140 kHz) with a 5% discrepancy.

The pure mechanical frequency response is also analyzed by ANSYS. Results (Figure 3.4) show that the natural frequency is 258 kHz, which matches the analytical result (263 kHz) with a 2% discrepancy.

Comparing Figures 3.3 and 3.4, we find that the peak deformation value for the pure mechanical model (0.268692E-05) is bigger than that in water (0.667360E-06). These results coincide with the fact that the water produces a damping effect while there is no damping effect for the pure mechanical case. Also we can notice that the frequency bandwidth is broader for the case in water. This coincides with the fact that the fluid flattens the frequency response of the diaphragm.

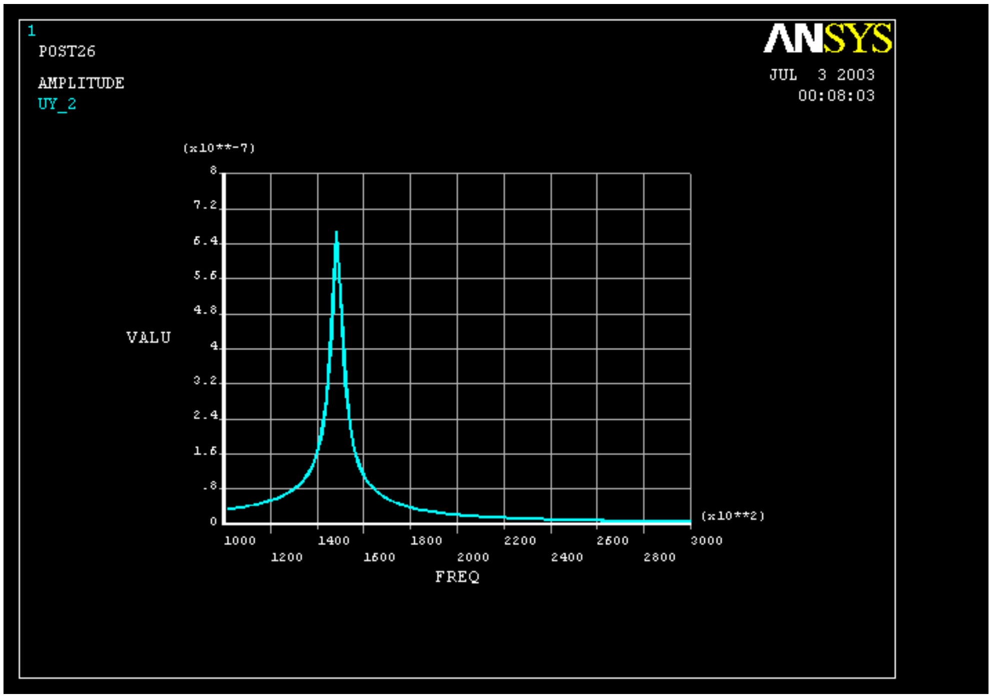

Figure 3.3, Frequency response of the diaphragm in water.

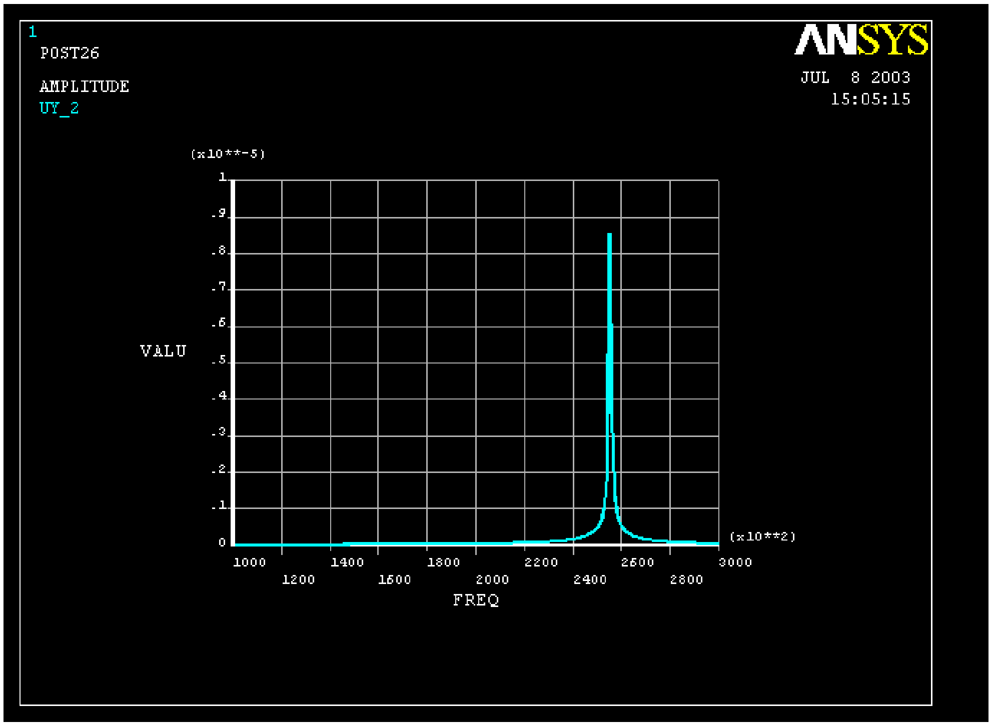

Figure 3.4, Pure mechanical frequency response of the diaphragm.

3.2.2 Three dimensional ANSYS model

3.2.2.1 Pure mechanical model

As mentioned before, when the angle between the propagation of the acoustic wave and the surface direction of the diaphragm is other than 0, the model is no longer axially symmetric and a three dimensional model has to be built. We first build a three dimensional model that is not immersed in fluid. Figure 3.5 shows the three dimensional model with a meshed diaphragm and a supporting tube. This time, double layer 4-node shell element shell63 is used to model both the diaphragm and the supporting tube. The degrees of freedom (DOFs) of the nodes along the diaphragm's edge and for all supporting tubing are set to 0 as boundary conditions.

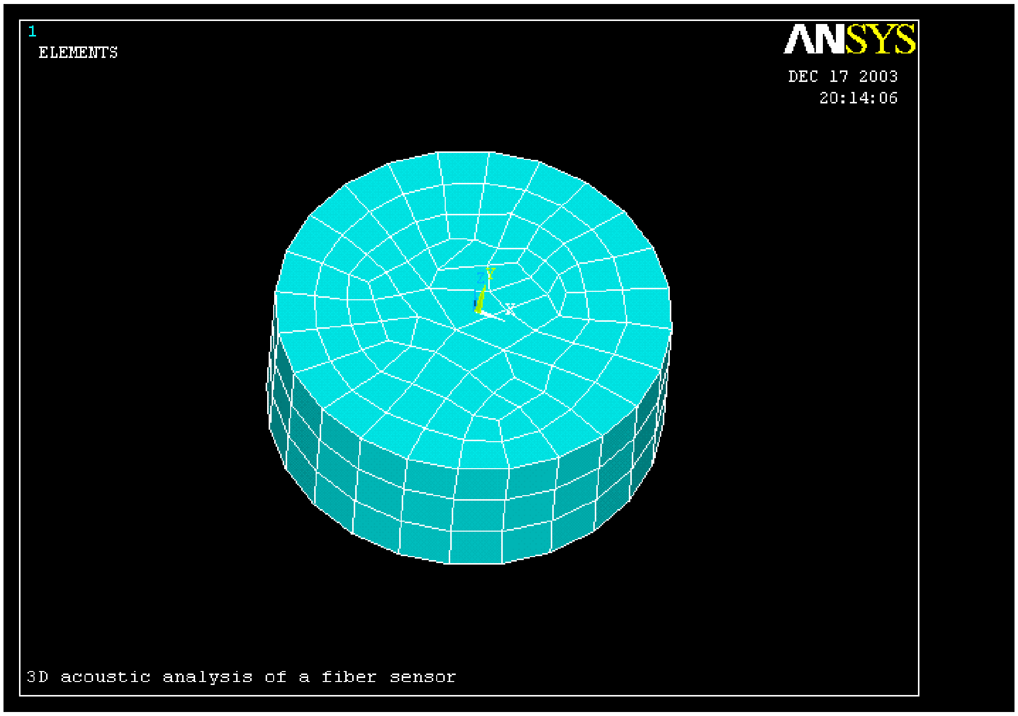

Figure 3.5, Meshed sensor diaphragm (upper surface) and supporting tube.

<u>Modal Analysis</u>

The modal analysis shows the lowest mode oscillating at 262.8 kHz. Figure 3.6 shows the mode shape.

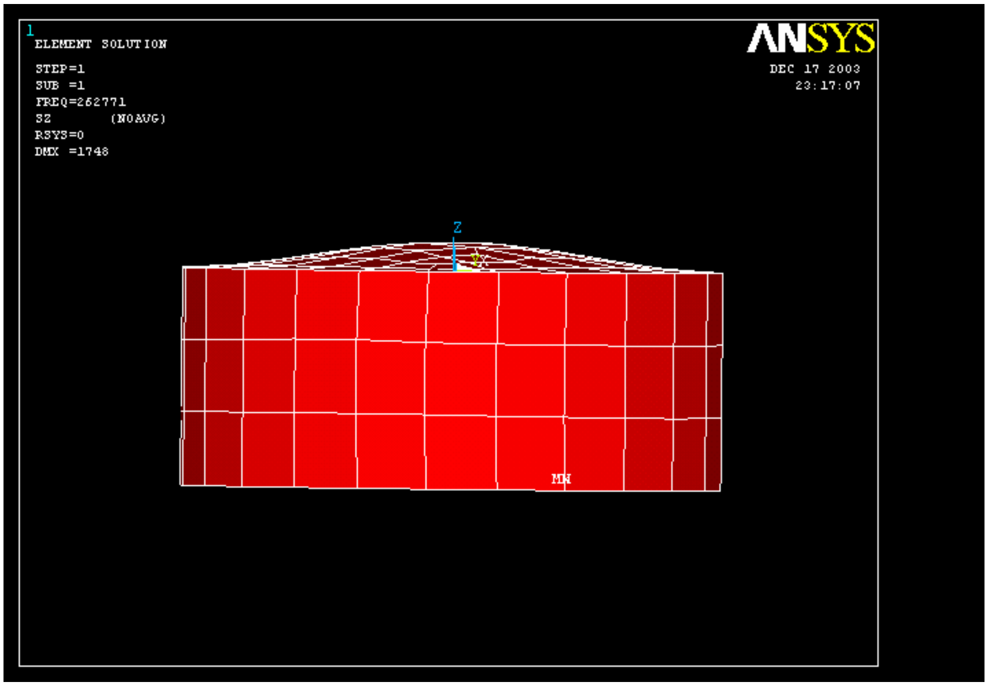

```
1
ELEMENT SOLUTION

STEP=1
SUB =1
FREQ=262771
SZ        (NOAVG)
RSYS=0
DMX =1748
```

```
DEC 17 2003
  23:17:07
```

Figure 3.6, The lowest order mode shape of the diaphragm.

Static analysis

Figure 3.7 is the contour plot of the deformation of the diaphragm when a mechanical pressure of 10000 Pa is applied to the surface of the diaphragm. The deflection in the center of the diaphragm is 0.0173 microns. From Equation 2.1, the maximum deflection of the diaphragm in the z direction is 0.018 microns. The results of ANSYS model show good agreement with the analytical results.

Harmonic analysis

Figure 3.8 shows the frequency response from 100 to 300 kHz when a sinusoidal mechanical pressure is applied to the diaphragm. The natural frequency is 262.7 kHz, which matches the analytical results (263 kHz) very well.

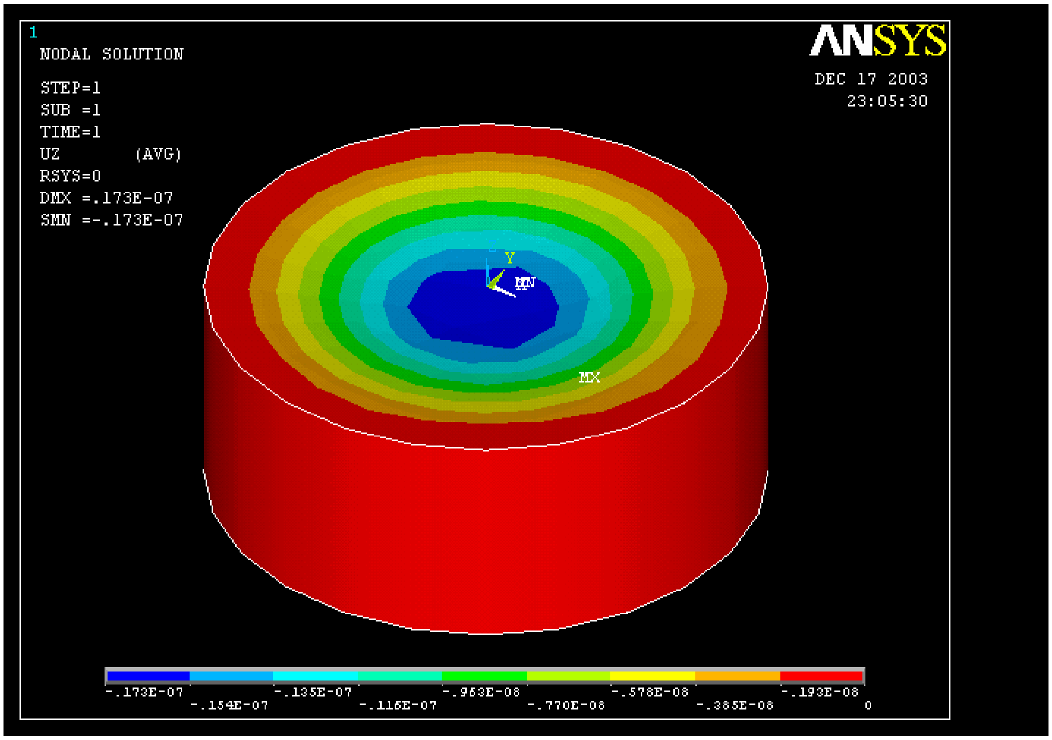

Figure 3.7, Contour plot of the deflection of the diaphragm.

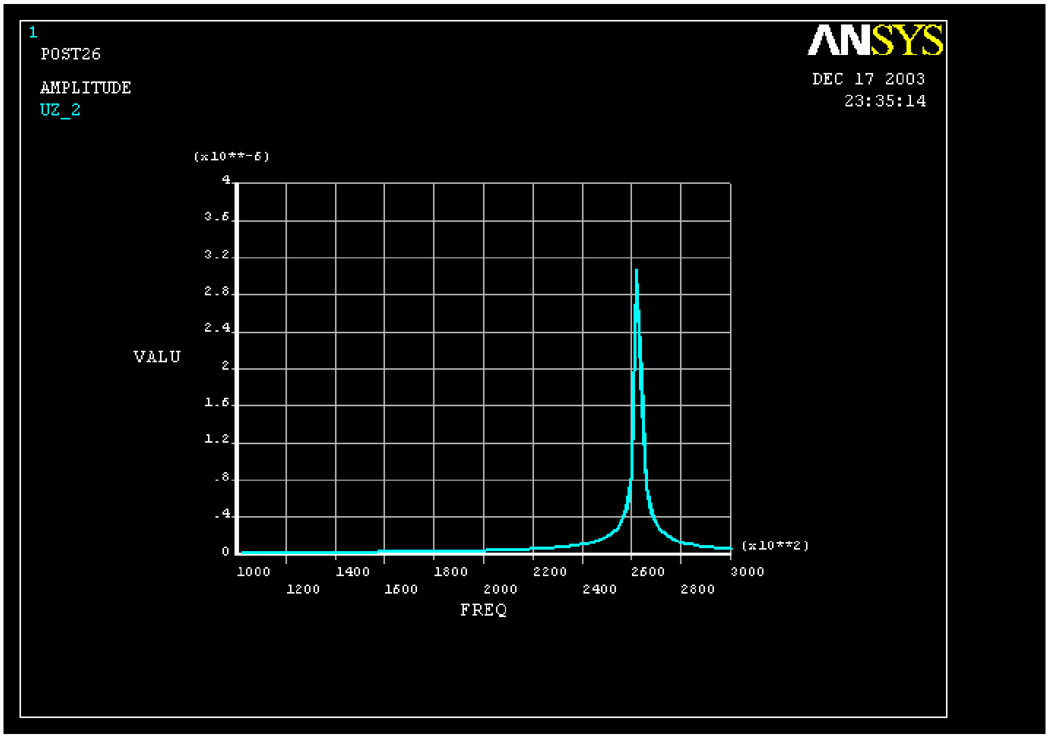

Figure 3.8, Results of harmonic analysis.

3.2.2.2 Sensor in fluid

The sensor in fluid model includes the parts in Figure 3.5 and a fluid region. The element type we used for the diaphragm and the supporting part of the sensor is still shell63. The acoustic element type for water is fluid30. For a simple structure analysis, the boundary of the fluid is λ away from the shell surface, where λ is the wavelength corresponding to the smallest frequency used for the harmonic analysis. Free meshing is used to mesh the whole fluid structure model. In order to get an accurate simulation model, quadratic 2-D elements are used for meshing element shell63 and quadratic hexahedral elements are used for meshing element fluid30. Even though this increases the complexity and the running time of the model, it is proven to increase the accuracy of the model. 15 divisions per wavelength are used for free meshing, which requires intervention in the free meshing. The fluid structure interface is set to the fluid30 element attaching the sensor shell elements. An absorption layer is formed along the outer side of the fluid cylinder as part of the boundary conditions. Further boundary conditions include constraining the degree of freedom of both rotations and displacements to 0 for both the diaphragm edge and the supporting part of the diaphragm. All DOFs of the other nodes on the diaphragm are not constrained. A double shell layer is used to isolating the outside of the sensor from the internal side of the sensor.

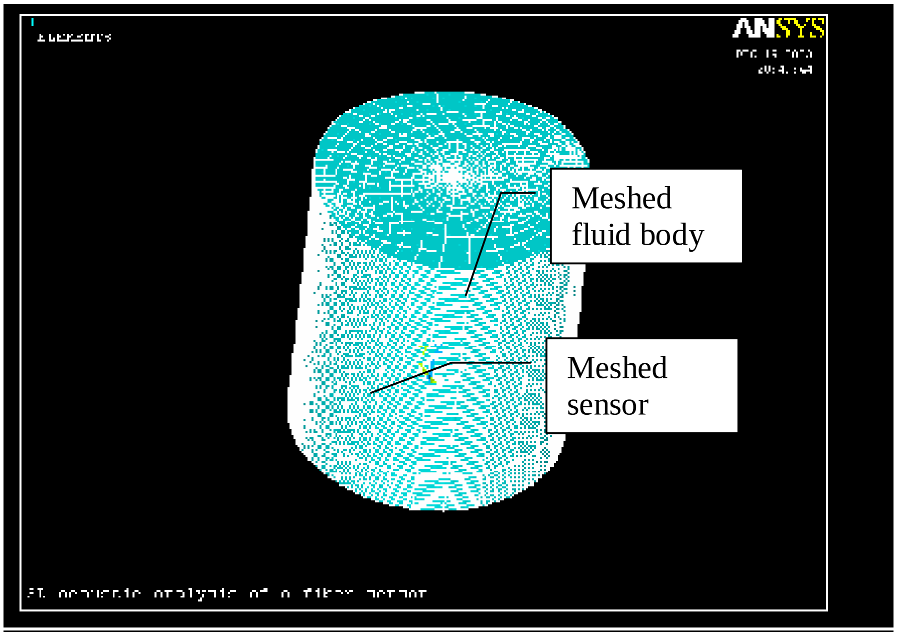

Figure 3.9, Three dimensional ANSYS model in fluid.

Harmonic analysis was performed from 100 to 300 kHz when a sinusoidal mechanical pressure of 10000 Pa is applied to the surface of the diaphragm. Figure 3.10 shows the results of the harmonic analysis. A natural frequency down shifted to 148 KHz is obtained in water, the same as the results of the two-dimensional case.

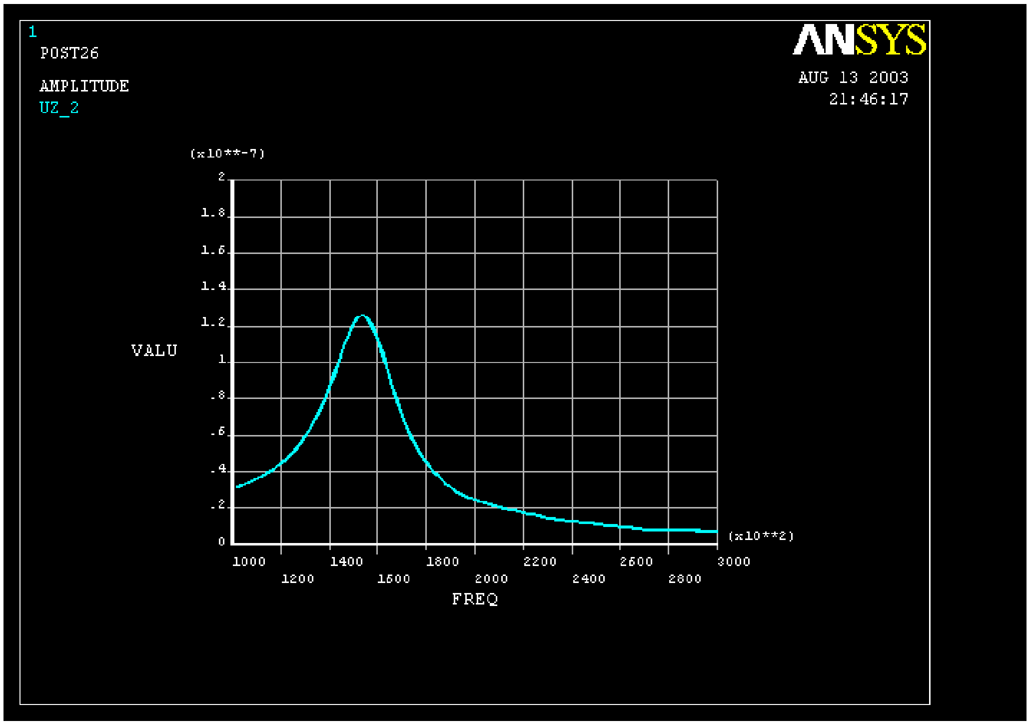

Figure 3.10 Frequency reponse from harmonic analysis.

3.2.2.3 Angular dependence of the frequency response

Harmonic analysis was performed from 110 to 300 kHz, under a sinusoidal acoustic wave of 10000 Pa. The acoustic wave is launched at 0, 5, 15, 20, 25, 30, 35, 40, 45, 50, 60, 70 and 80 degrees to the surface of the diaphragm, respectively. The testing frequencies range from 110 kHz to 300 kHz which are the frequency ranges of interest for PD detection. The results of the angular dependence of the frequency response of the sensor from the ANSYS model are shown in Figure 3.11. Figure 3.12 shows the angular dependence of the frequency response for 160 kHz and 180 kHz. The 3dB range is approximately ±50 degrees.

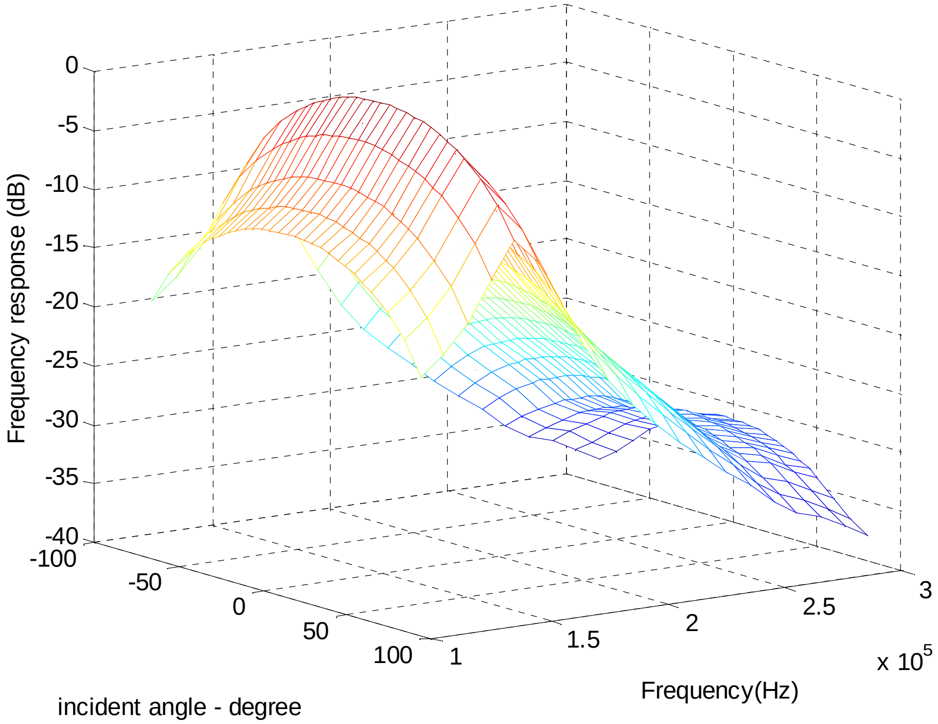

Figure 3.11, Angular dependence of frequency response of the sensor.

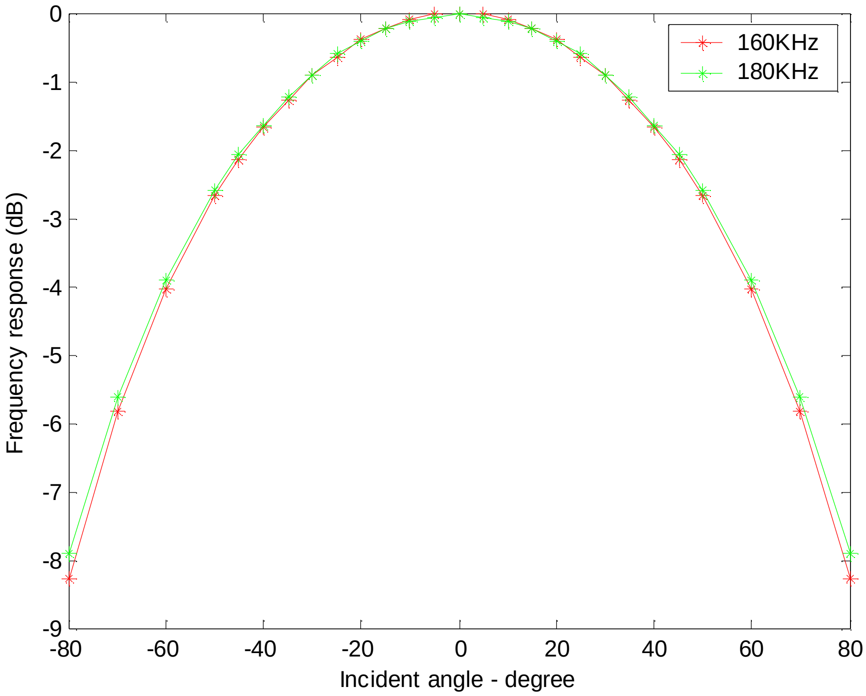

Figure 3.12, Angular dependence the sensor for frequencies at 160 kHz and 180 kHz.

3.2.3 Comparison of the Ansys results with theory

There are three models for the angular dependency of the diaphragm, namely, a piston in rigid baffle model, a piston in a soft baffle and an unbaffled piston. The far field angular dependence of the radiated pressure for a circular piston in a rigid planar baffle is given by P. M. Morese [6] and David G. Shombert [2].

$$p(r,q) = p(r)\left(\frac{2J_1(ka\sin q)}{ka\sin q}\right) \tag{3.4}$$

where $J_1(ka\sin q)$ is the first order Bessel function, k is the wave number, a is the piston radius, r is the distance from the center of the piston to the field point, and q is the angle between r and the piston axis.

Considering the plane acoustic wave, the pressure is not a function of r. Also considering a linear relationship between the deflection and the pressure, the angular dependence of the deflection will become:

$$z(q) = z_0\left(\frac{2J_1(ka\sin q)}{ka\sin q}\right) \tag{3.5}$$

where z is the deflection of the diaphragm and z_0 is the maximum deflection for $q = 0$.

The second model called a soft baffle model was suggested by Selfridge, in which the angular dependence is modified by an additional cos(q) term. In this case, the theoretical response would be

$$z(q) = z_0\left(\frac{2J_1(ka\sin q)}{ka\sin q}\right)\cos q \tag{3.6}$$

The third model called piston in free space, also known as un-baffled piston, was suggested by Delannoy. The response of this model is

$$z(q) = z_0 \left(\frac{2J_1(ka\sin q)}{ka\sin q} \right) \left(\frac{1+\cos q}{2} \right) \tag{3.7}$$

These three directivity patterns are shown in Figure 3.13, for 160 kHz with a wave velocity of 1480m/s, a = 1.25 millimeter. Figure 3.13 also includes the angular dependence obtained from the ANSYS model for 160 and 180 kHz for comparison. The ANSYS results are much like the soft baffle model.

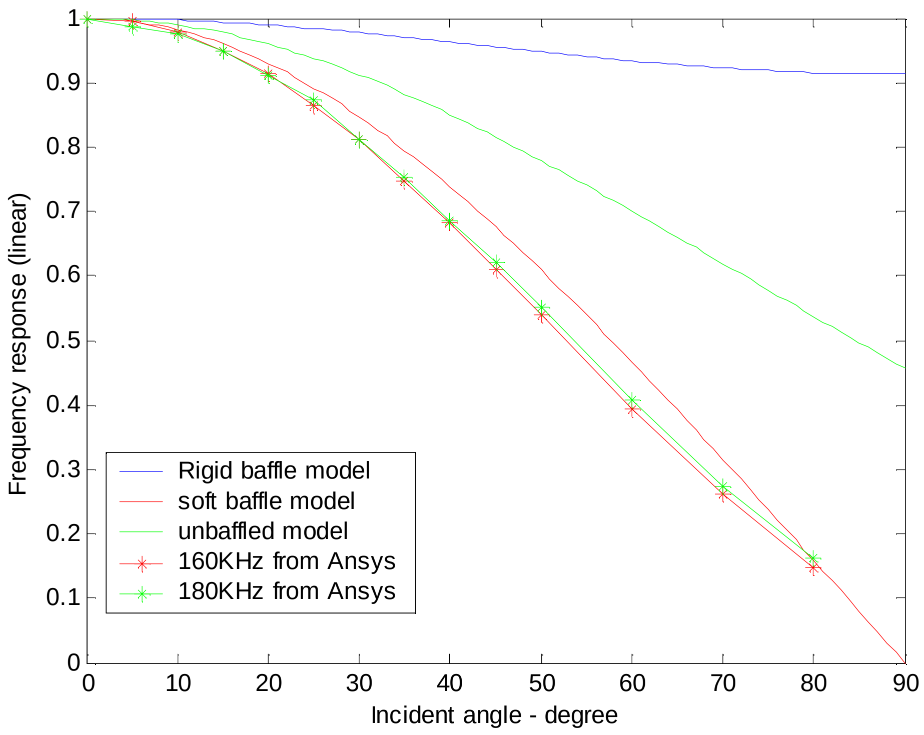

Figure 3.13, Directivity patterns for a piston in a rigid baffle, a piston in a soft baffle and an unbaffled piston.

3.3 Experiments for angular dependence of the frequency response

3.3.1 Basic idea

Figure 3.14 is the block diagram of the principles for the transfer function measurement. The acoustic wave generated by the ultrasonic transducer is expressed as $X_{input}(f)$. The source wave travels through the water and other environments (transfer function $H_{path}(f)$) until it reaches the PZT detector ($H_{PZT}(f)$) or the fiber sensor ($H_{sensor}(f)$).

The final output is $Y_{PZT}(f)$ for the PZT detector and $Y_{sensor}(f)$ for the fiber sensor. The input-output relationship is

$$Y_{PZT} = X_{input} H_{path} H_{PZT} \tag{3.8}$$

$$Y_{sensor} = X_{input} H_{path} H_{sensor} \tag{3.9}$$

Dividing equation (3.9) by equation (3.8), we have

$$H_{sensor} = \frac{Y_{sensor}}{Y_{PZT}} H_{PZT} \tag{3.10}$$

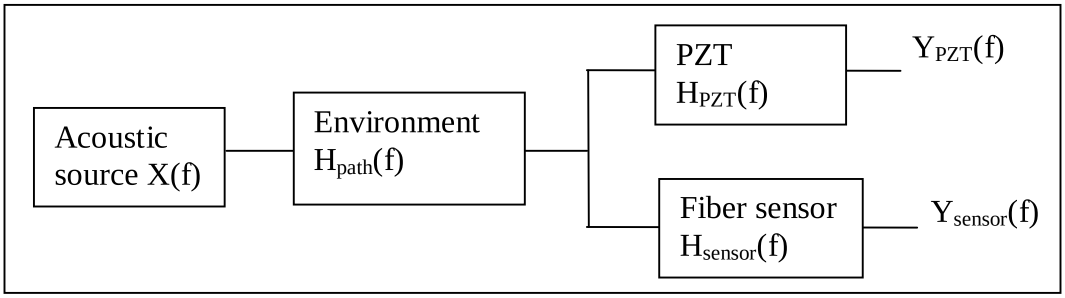

Figure 3.14, Block diagram of the transfer function measurements.

Experimentally we can measure Y_{sensor} and Y_{PZT}, and we know H_{PZT} from the factory specifications. We can therefore obtain

$$H_{sensor} = Y_{sensor} - Y_{PZT} + H_{PZT} \text{ (dB).} \tag{3.11}$$

3.3.2 Experimental setup

Figure 3.15 is a schematic diagram of the experimental setup. An ultrasonic source (Physical Acoustic Corporation, PAC WDU) is attached to a frame immersed in a tank filled with water. The acoustic source is driven by a pulser (PAC, HV-101). A fiber acoustic sensor fixed in a sensor holder is placed 410 millimeters away from the acoustic source. The angle between the source and the sensor is controlled by a rotator. In order to minimize the effect of multiple reflections between the sensor and the source, the center of the ultrasonic source is 30millimeters higher than the center of the acoustic fiber sensor. The signals from the sensor are processed in an oscilloscope (LeCroy, LT322 500 MHz) after passing through a Q point tuning system. Figure 3.16 shows all the connections required for the experiments. The tank with the frame, the sensor holder, the rotator and the sensors is shown in Figure 3.17.

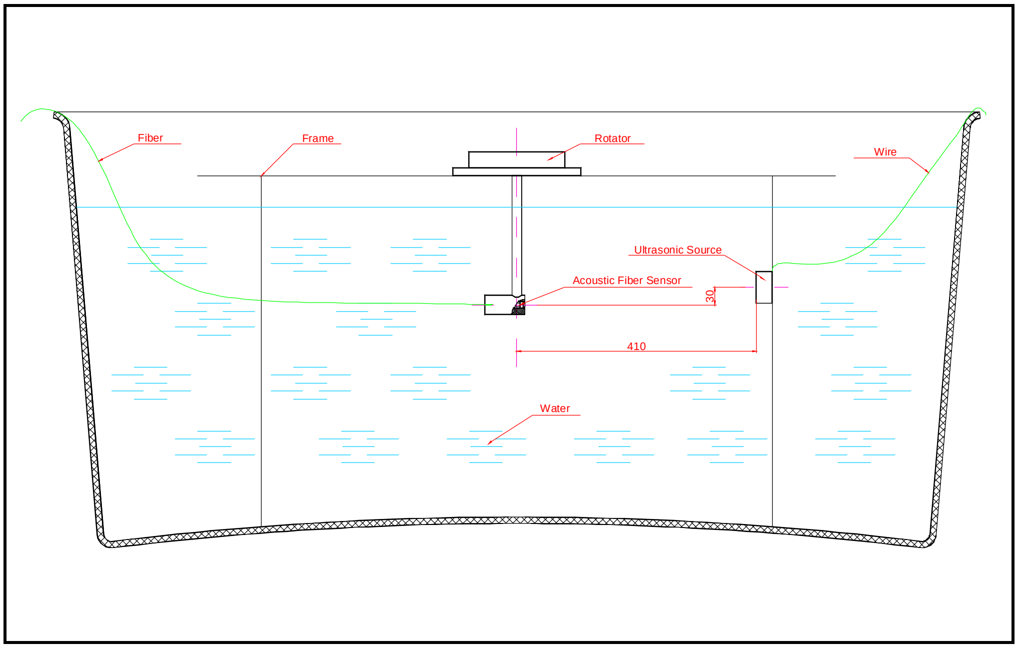

Figure 3.15, Schematic diagram of experimental setup.

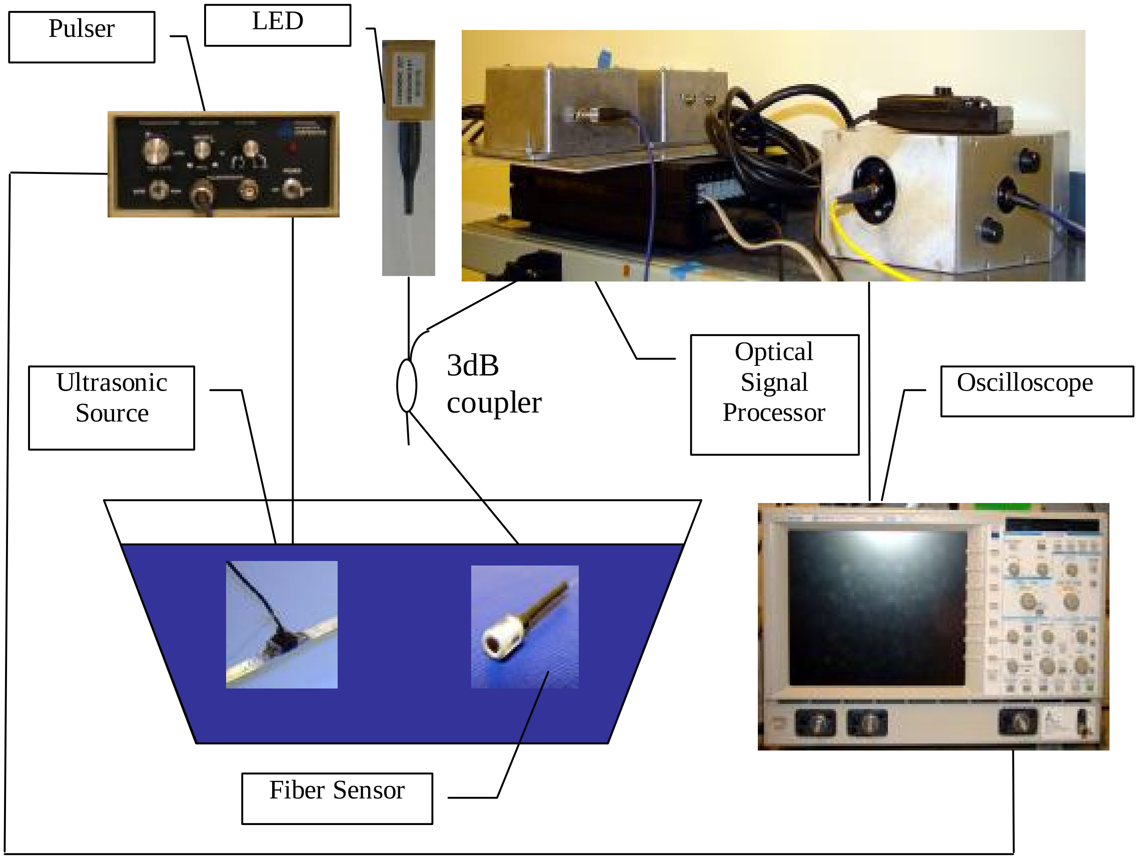

Figure 3.16, Connections of experimental setup for angular dependence of the frequency response.

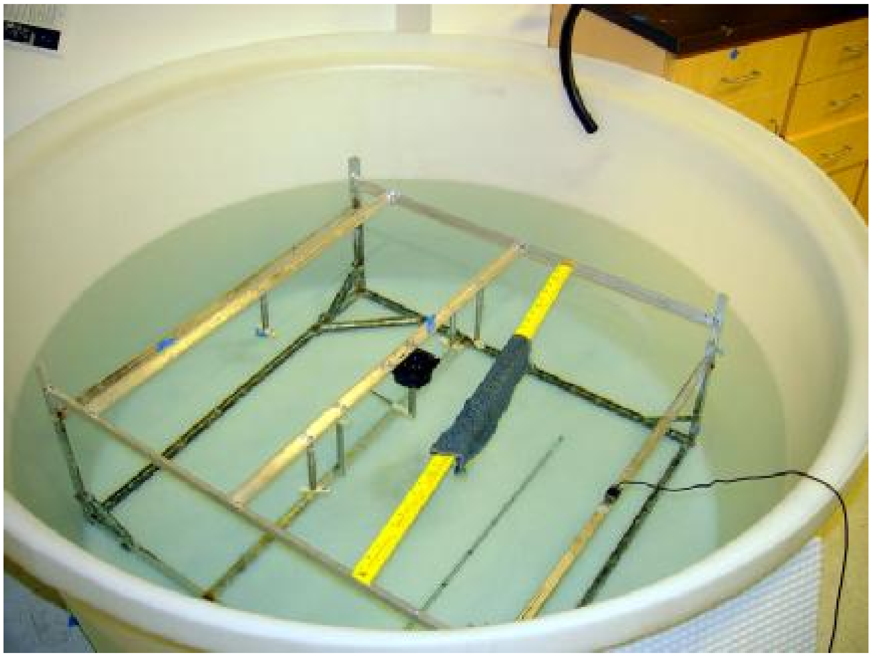

Figure 3.17, Realistic experiment outlook inside tank.

3.3.3 Experimental Results

After sampling the waveform of the detected signal with an oscilloscope, we can use the FFT method to find the spectrum of the received signals. Before we process the frequency response of the sensor, we need to make sure that the received signal from both the fiber sensor and the PZT detector do not include multi-path interference. Figure 3.18 is an example of a received signal with multi-path interference. The waveform between the two red dashed lines is the main signal. Other waveforms outside of the red dashed lines are due to multi-path interference. In order to get the correct frequency response of the sensor, we need to either block the multipath interference or only process the main received signal from either the sensor or the PZT. In this experiment we blocked the multi-path interference. In order to reduce the AWGN noise components, we sampled the waveform 20 times and averaged the sampled waveforms. Then we Fourier transformed the signals to obtain the spectra of the signals. Because we already knew the frequency response of the PZT sensor, by using equation (3.11), we can get the frequency response of the optical sensor. Figure 3.19 shows the amplitude frequency response of the optical sensor (black trace) determined using this method.

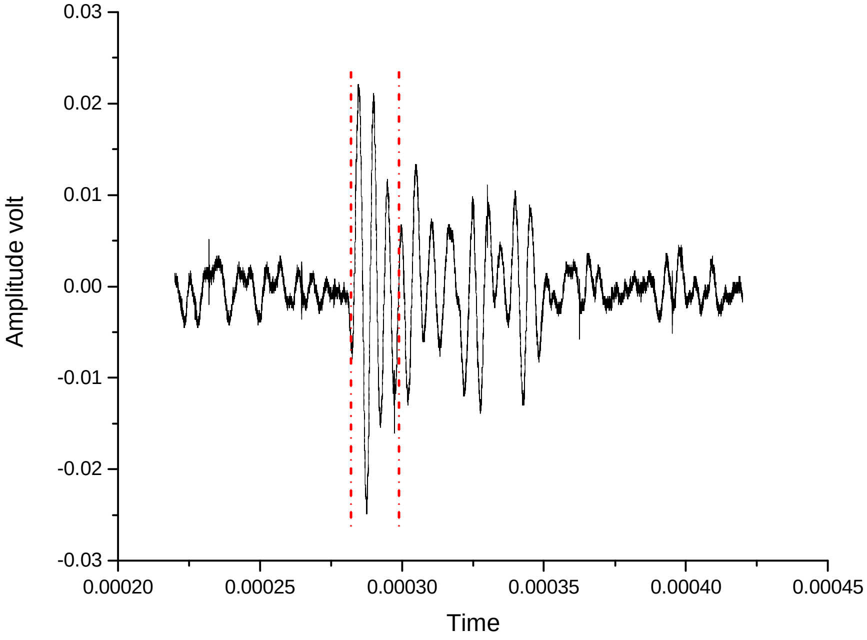

Figure 3.18, Received signal from sensor with multi-path interference.

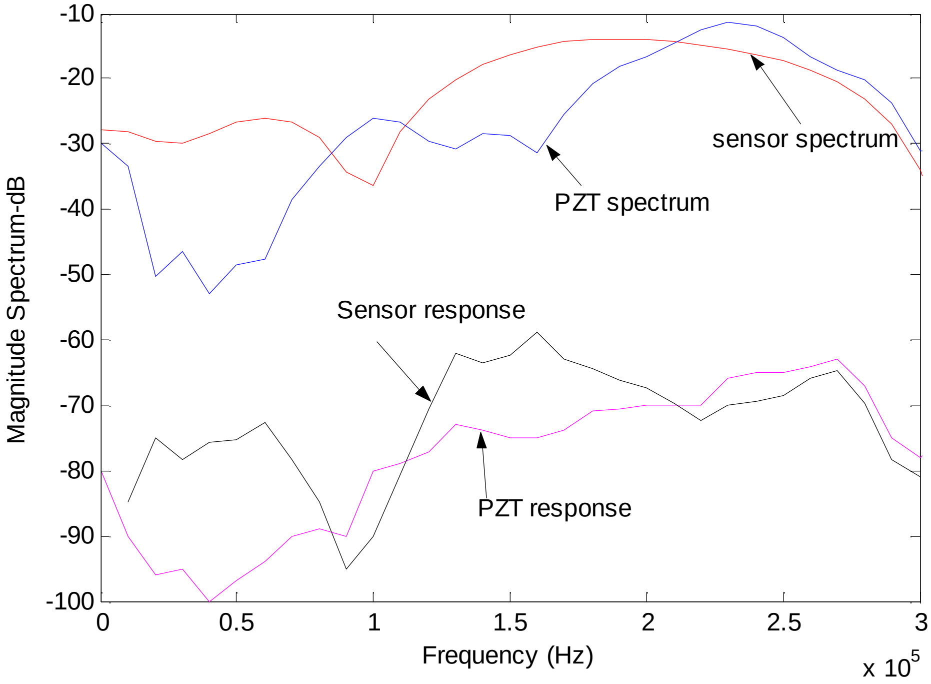

Figure 3.19, Sensor frequency response for 0 degree incidence.

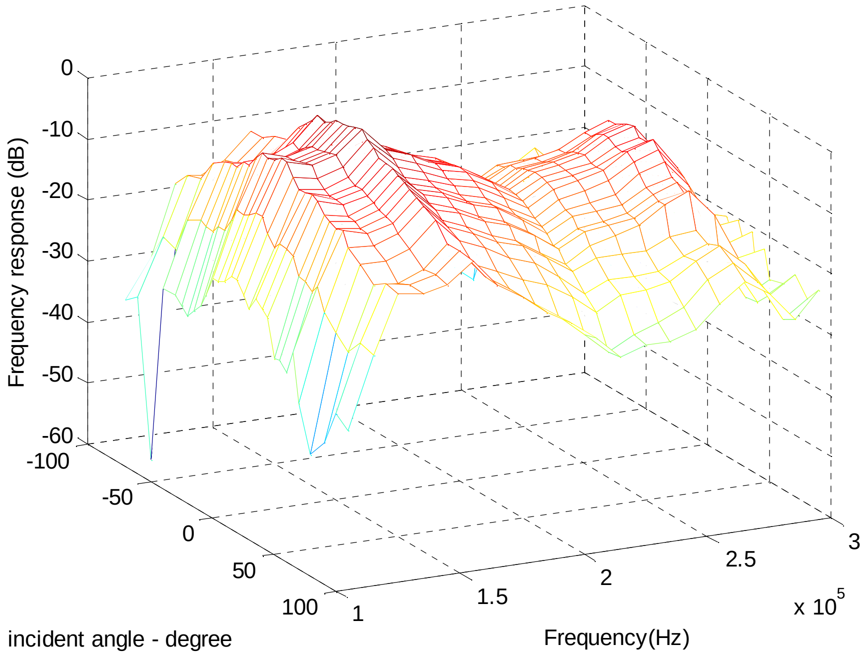

Figure 3.20, Angular dependence of the frequency response.

Repeating the procedure from 0 to ±90 degree incidence, we can get the frequency response of the sensor for different incident angles. Figure 3.20 shows the results of the angular dependence of the frequency response of the sensor in the range 110 kHz to 300 kHz. In this figure, we normalized the maximum response as 0dB. The center frequency of the sensor in the water is around 160 kHz. In order to find the exact angular dependence of the frequency response of the sensor, we sliced Figure 3.20 at two frequencies, 160 kHz and 180 kHz. These angular dependences are shown in Figure 3.21. The red curves in Figure 3.21 are fitted Lorenz curves to smooth the data. At 160 kHz, the 3dB angular range of the sensor is about 60 degrees, and at 180 kHz, the 3dB angular range is about 80 degrees. Considering the ±45 degree range of incidence around 160 kHz, the signal exhibits a 5 dB loss due to incident angle at 45 degree. Therefore, the received signal strength will vary 5dB within this ±45 degree range. These results are approximately 3 dB narrower than what we obtained from the ANSYS model. In the ANSYS model, we were only interested the deflection of the diaphragm. In this section, we considered the whole sensor system, including the optical system, the Q point tuning system, the electrical amplifier and the electrical filters. The whole system is not a strictly linear system. Moreover, the method used to assemble the diaphragm may affect the angular dependence of the sensor. All these factors may reduce the bandwidth of the angular response.

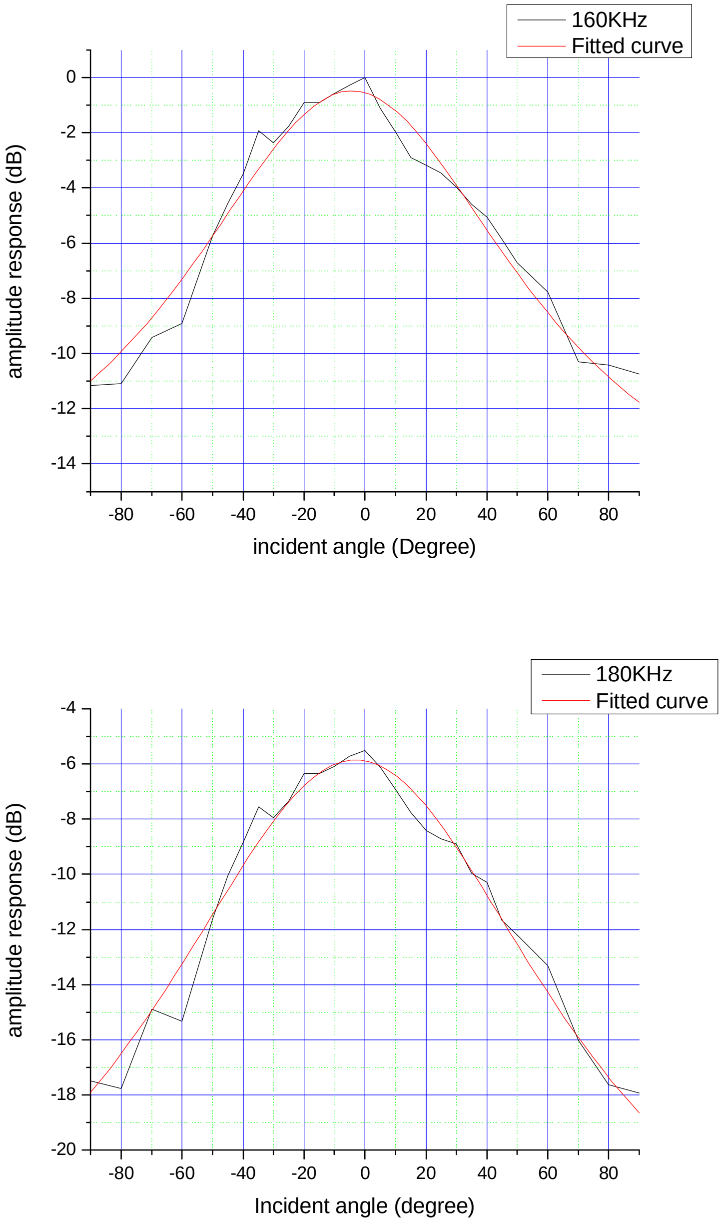

Figure 3.21, Angular dependence of the frequency response of the sensor at 160 kHz and 180 kHz.

Considering the sensor array layout in Figure 2.1, where each corner has one sensor to monitor the unit, when we design the sensitivity of the sensor, we actually need to satisfy a sensitivity that is 5dB higher than the sensitivity estimated using Equation (2.1) in order for the sensor system to be able to monitor the whole unit. If the sensor's sensitivity cannot meet the requirements, more sensors are needed to successfully monitor the unit. If we would like the sensor to detect a 0.2Pa acoustic wave 2 meters away with a good signal to noise ratio, we would like the sensor to have a sensitivity 5 to 6 dB higher. This means that the sensor should be able to detect a 0.05Pa acoustic wave with the same signal to noise ratio. Considering a 8×8×8 meter^3 transformer, we can divide the tank into eight 4×4×4 meter^3 cubes. Each cube will need 8 sensors. Therefore a total of 64 sensors are needed in the transformer. This configuration can also avoid blocking by the windings inside of the transformer. The required signal to noise ratio is determined by the position location accuracy we will discuss in Chapter 4. Also the signal to noise ratio is not only determined by the sensor head, but also by the signal processing unit following the sensor detection system.

3.4 Conclusion

In this chapter, a two dimensional and a three dimensional ANSYS models were successfully built to analyze the performance of the EFPI sensors used for PD detection. The angular sensitivity of the sensor is given based on the three dimensional model. The results of this angular dependence closely match the soft baffle model. An experiment was conducted in the lab to determine the angular dependence of the frequency response of the sensor. A ±45 degree monitoring angle range was found to exhibit an amplitude frequency fluctuation of 5dB. Based on these results, an optimized sensor array layout is to place the sensors in the corners of a transformer. When the received signal to noise ratio cannot be met, the transformer tank can be divided into several sub-cubes. The adverse result is that we have to increase the number of sensors for the system.

References:

1. Zhao Zhiqiang, Mark MacAlpine, and M. Süleyman Demokan, “The Directionality of an Optical Fiber High-Frequency Acoustic Sensor for Partial Discharge Detection and Location”, Journal of Lightwave Technology, vol. 18, no. 6, pp. 795-806 , 2000.
2. David G. Shomber, Stephen W. Smith, and Gerald R. Harris, “Angular response of miniature ultrasonic hydrophones”, Med Phys, vol. 9(4), pp. 484-492, 1982.
3. Jochen F. Frucker, Alexander Eisenberg, Martin Krix, Ralf,Lotsch, Martin Pessel, and Hans-Georg Trier, “Rigid piston approximation for computing the transfer function and angular response of a fiber-optics hydrophone”, J. Acoust. Soc. Am. vol. 107(4), pp. 1994-2003, 2000.
4. Wieland Weise, Volker Wilkens, and Christian Koch, “Frequency response of fiber-optic multilayer hydrophones: experimental investigation and finite element simulation”, IEEE Transactions on ultrasonics, ferroelectrics, and frequency control, vol. 49(7), pp. 937-945, 2002.
5. ANSYS 7.0 online documents
6. P. M. Morese and U. K, Ingard, in Theoretical Acoustics, McGraw-Hill, New York, 1968.

Chapter 4 Position Location of Partial Discharges

Because different PD sites have different components, successfully locating a PD source can help identify the problem in the transformer. Also, precisely locating a PD source is very useful for transformer maintenance and repair. However, accurate PD location is not easy due to complex transformer structures, which may obstruct the path between the PD sites and the sensor terminals, or distort the PD waveforms. A sensor array layout is proposed in Chapter 2 to avoid obstacles in the transformers. Also, attenuation of PD waves and multipath interference are two other impairments that degrade the position accuracy because they can reduce the signal to noise ratio of the received signals [1, 2]. Lazarevich's thesis [2] described the determination of partial discharge locations using a convolution method. However, there are several aspects that need improvement in her experiments. First, the PD detection range should be increased. Her experiment was carried out in a 10-gallon aquarium. The distances between the acoustic source and the sensors ranged from 7.2 to 13.5 centimeters. Second, the position accuracy needs to be improved. In the experiment, Lazarevich defined a 10-centimeter error cube. Although her 11 tested data sets fell in this error cube, she ignored received signals with a signal to noise ratio less than 14dB in order to maintain all position data within this defined error cube. We need to collect large amount of data to evaluate the position results statistically. Finally, a predefined 10-centimeter cube for a range of only 7.2 to 13.5 centimeter seems too big. This chapter will focus on solving these two problems.

In this chapter, the triangulation algorithm using hyperbolic position fixing based on time difference of arrival (TDOA) is first introduced. Then three methods, convolution, leading edge with FIR filtering and correlation are used to determine the TDOAs. Results show that the cross-correlation and leading edge with FIR digital filter methods have the better positioning accuracy than the convolution method. Finally we demonstrated that 94.48% of the positioning data is bounded by a $35.1\times9.8\times51.1\ \mathrm{mm}^3$ cube using the cross-correlation method, and 100% of the positioning data is bounded by a $22.7\times4.1\times5.3\ \mathrm{mm}^3$ cube using leading edge with FIR filters, with a sensing range of 810 mm in a 500 gallon water tank. These positioning results indicate that the best sensor array layout is to spread the sensors in the tank in order to increase the positioning accuracy.

4. 1 Positioning Algorithm

The algorithm for locating a PD source is a hyperbolic position fixing solution based on the time difference of arrival (TDOA) [1]. When a number of spatially separated sensors capture the emitted signals and the time difference is determined, the emitter location can be calculated. The range between the source and the sensor can be expressed as

$$r_1^{\,2} = (x - x_1)^2 + (y - y_1)^2 + (z - z_1)^2 \tag{4.1}$$

where (x, y, z) are the coordinates of the source and (x_1, y_1, z_1) are the coordinates of the sensor. For each sensor in an array, one of these spherical equations can be written and a system of nonlinear equations is created.

If the range is written as the speed of sound in the medium times the signal propagation time, then the difference equation can be written in terms of a time difference between two sensors. This leads to a system of linear equations that relates the source coordinates to the unknown range from the first sensor to the source,

$$\begin{bmatrix} x \\ y \\ z \end{bmatrix} = -\begin{bmatrix} x_{21} & y_{21} & z_{21} \\ x_{31} & y_{31} & z_{31} \\ x_{41} & y_{41} & z_{41} \end{bmatrix}^{-1} \times \left\{ \begin{bmatrix} r_{21} \\ r_{31} \\ r_{41} \end{bmatrix} r_1 + \frac{1}{2} \begin{bmatrix} r_{21}^{\,2} - K_2 + K_1 \\ r_{31}^{\,2} - K_3 + K_1 \\ r_{41}^{\,2} - K_4 + K_1 \end{bmatrix} \right\} \tag{4.2}$$

where (x_{i1},y_{i1},z_{i1}) is the difference between the coordinates of the *i*th sensor and the first sensor, r_{i1} is the speed of sound in the medium times the time difference found between the first and the *i*th sensor, r_1 is the range from sensor 1 to the source, and $K_i = x_i^2 + y_i^2 + z_i^2$. If each of the source coordinates (*x*, *y*, *z*) is solved in terms of r_1, the resulting expressions can be inserted in the range equation for sensor 1 (Eq. (4.1)) in order to solve for r_1. Once the positive root of the quadratic equation is determined, the value of r_1 can be used in Eq. (4.2) to determine the source coordinates.

4.2 PD location experiments using different methods

4.2.1 Experimental setup

The experimental setup is the same as described in Chapter 3, but with four sensors monitoring the acoustic source. Figure 4.1 shows the coordinate systems of the four sensors and the acoustic source, with x, y and z values (in millimeter) for sensor #1 of (433.9, 186.1, 306.0), sensor #2 of (537.7, 209.4, 404.6), sensor #3 of (542.0, 457.6, 392.7), sensor #4 of (420.1, 697.5, 302.5) and the acoustic source of (8.4, 446.1, 409.3). Figure 4.2 shows the samples of the oscilloscope waveforms from the four sensors. The blue stars in Figure 4.2 indicate the peaks of the waveforms.

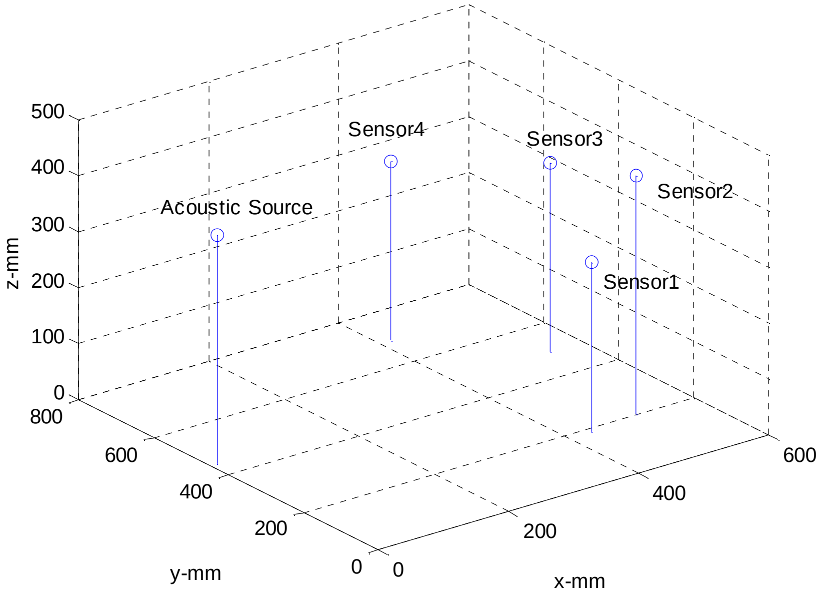

Figure 4.1, Coordinate system with four sensors and one acoustic source.

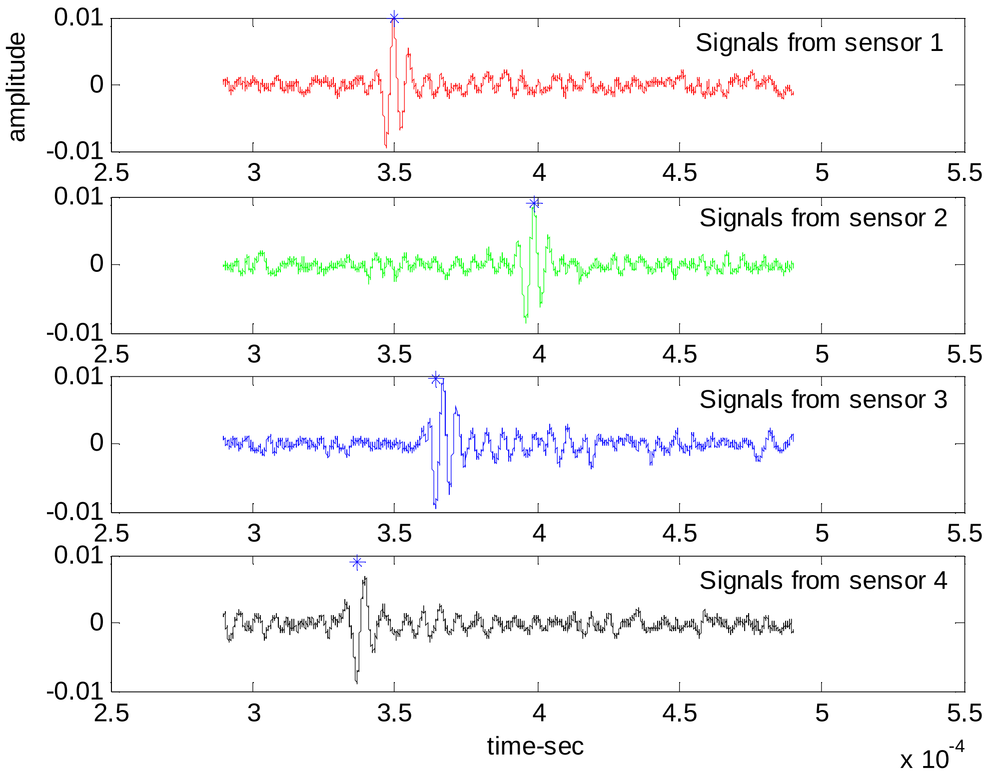

Figure 4.2, Detected acoustic waveforms at each sensor.

4.2.2 Effects of AWGN noise and multi-channel interference

A number of positioning simulations in the presence of additive white Gaussian noise source (AWGN) have been performed [2]. When the signal to noise ratio is poor, the positioning results will become inaccurate and will randomly change from time to time.

Figure 4.3 shows two sampled waveforms from Sensor 1. As can be seen, the maximum values of the two samples are different, and have a half wave delay. This half wave delay (2.668 microseconds) corresponds to 4 millimeter difference. When this error is used in the positioning program, we may get significant errors. Also from Figure 4.3, we can see the small oscillating fluctuations, which is from multi-path interference. When this multi-path interference is overlapped with the detected signal, the interference between multi-path signals will make the detected waveform fluctuate dramatically.

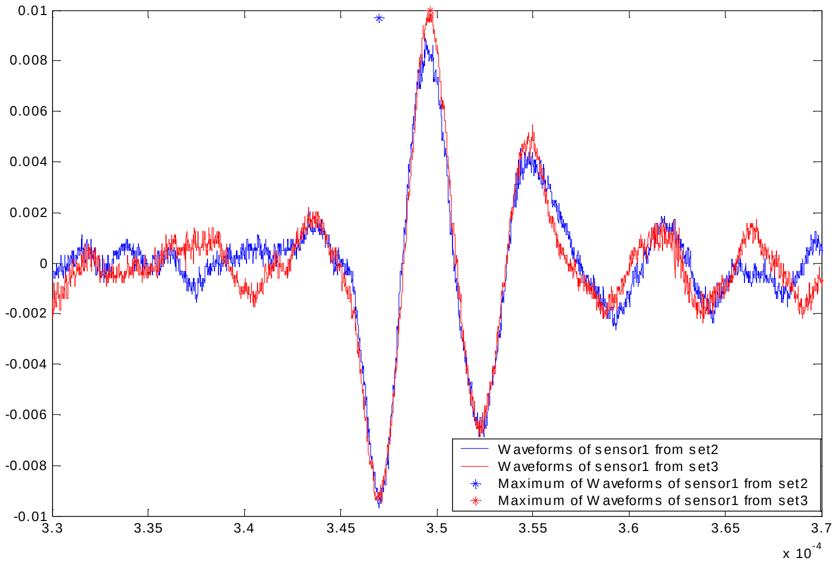

Figure 4.3, Two different samples of the detected acoustic waveforms from sensor 1.

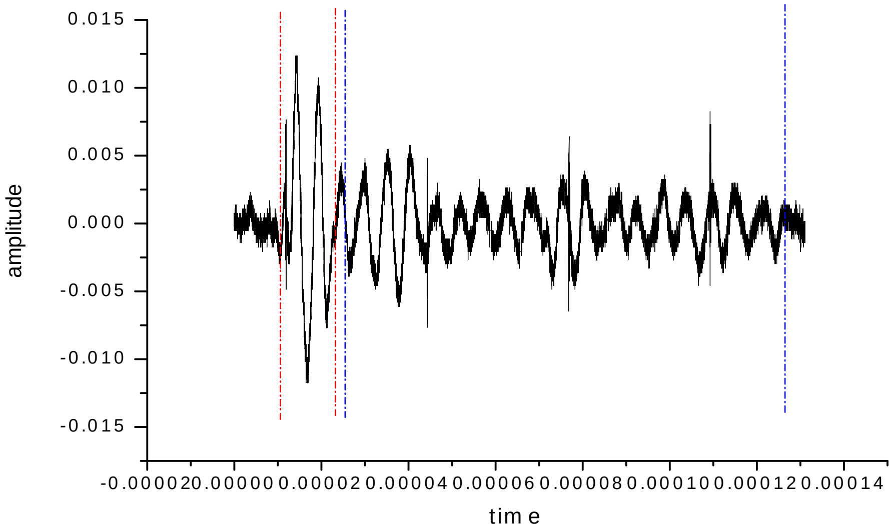

Figure 4.4, Multi-path interference signals

Another effect of multi-path interference may occur when the multi-path interference signals do not overlap with the desired line of sight (LOS) signal, as shown in Figure 4.4. In this figure, the signals between the two red dashed lines are the line of sight signals. The signals between two blue dashed lines are the multi-path interference from the reflection of the wall of the container and from the surface of the fluid. These multi-path signals will affect the accuracy of the timing of the detected signals from different sensors when we use the convolution or cross-correlation method to find the time delays. This inaccuracy will finally introduce errors for positioning. Therefore measures have to be taken to avoid this multi-path interference.

4.2.3 PD location using convolution method

Convolution functions basically as an integrator or a low pass filter. If the signals were identical and we consider only the AWGN noise channel, convolution functions as a matched filter. The output from the matched filter will reach maximum when the delay between the two signals is zero. Using this method we can determine the time delays for the four different sensors. Figure 4.5 shows the convolution of the signals of sensor k (k = 2, 3, 4, 1) with the signals from sensor 1. Using the TDOA routine, we can thus determine the PD location. Figure 4.6 shows the positioning results for 5 different measurements.

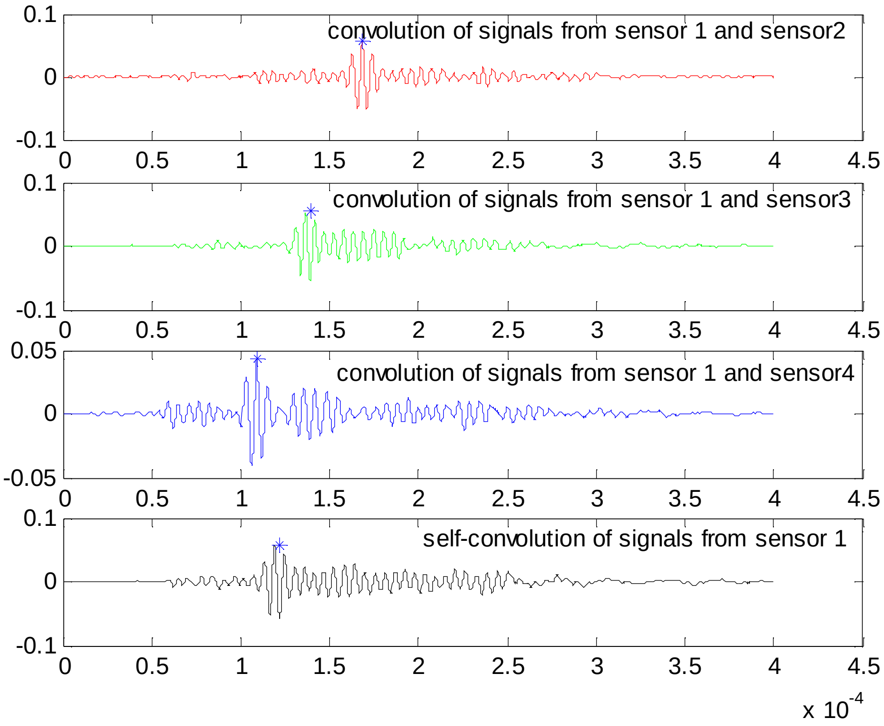

Figure 4.5, Convolution of the waveforms between sensor k (k = 1,2,3,4) and sensor 1.

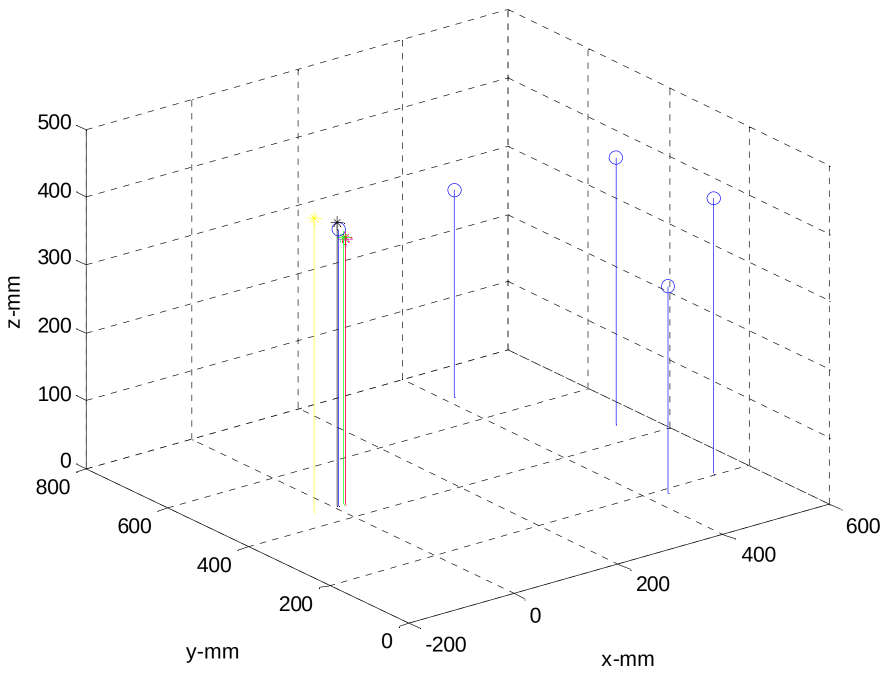

Figure 4.6, Positioning results using convolution method.

4.2.4 PD location using cross correlation method

The convolution method can be used to estimate the time delay of the received signals from two different sensors. However, this matched filter method cannot give the best estimate of the time delay between the two signals when the signals are corrupted by noise. Cross correlation is widely used to compare the similarities of the two signals. For an even function, cross-correlation and convolution are identical operations since flipping an even function prior to convolution has no effect. The cross-correlation is the largest when the lagged version of a function is most similar to the other function. Then, the products of the two functions are more positive. Where the products have both positive and negative results, integration yields smaller cross-correlation values. For perfectly uncorrelated, random functions, the cross-correlation is zero. The cross-correlation process incrementally slides the reference waveform over the signal being processed looking for a matching signal. Signals that are not related to the reference waveform result in a correlation value of 0. If a matching signal is found the correlation value increases to a maximum value for a perfect match and a minimum value for a matching but inverted wave. This property is very useful in determining the time delay when one detected signal has an inverted phase. From the above analysis, we could expect that cross-correlation could be better in finding the time delay of the received signals for two different sensors than using the convolution method, if the PD signals are not severely distorted at two different sensors during transients. The lag time at the maximum value of the cross correlation is the time delay between the two sensors. Figure 4.7 shows the cross-correlation of the signals of sensor k (k = 2, 3, 4, 1) with the signals from sensor 1. Using the TDOA routine, we can thus determine the PD location. Figure 4.8 is the positioning results for 5 different measurements. These five measurements are the same as in section 4.2.3 in which convolution method was used. The five positioning results are clustered in the red star because of the resolution of the picture. Table 4.1 shows the detailed positioning results.

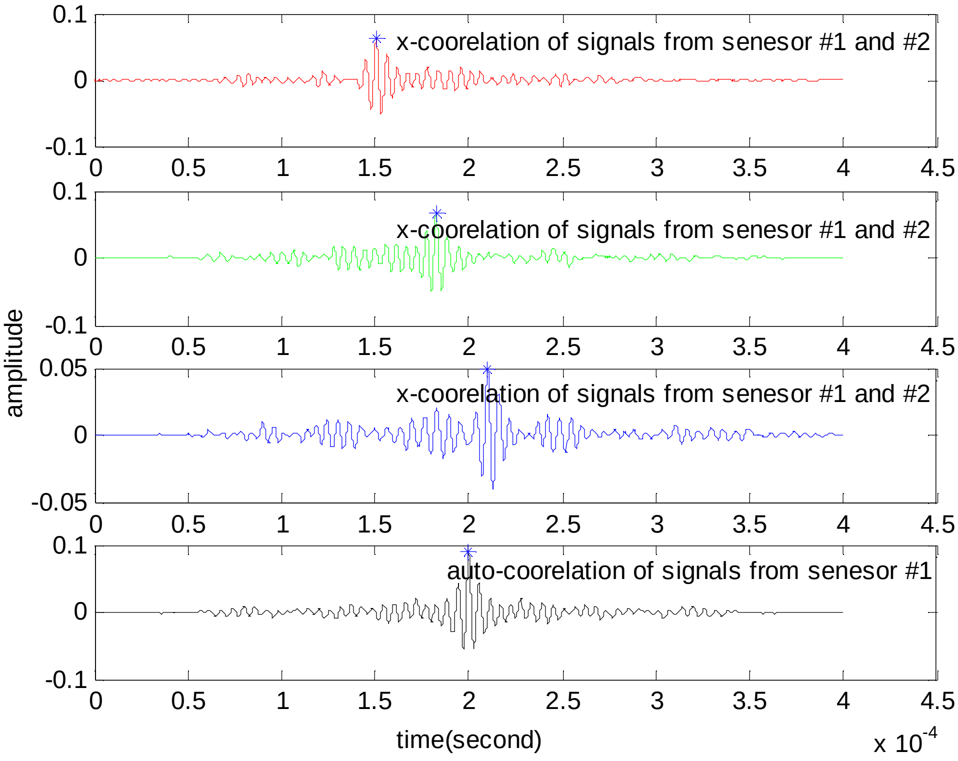

Figure 4.7, Cross-correlation the waveforms between sensor k (k = 1,2,3,4) and sensor 1.

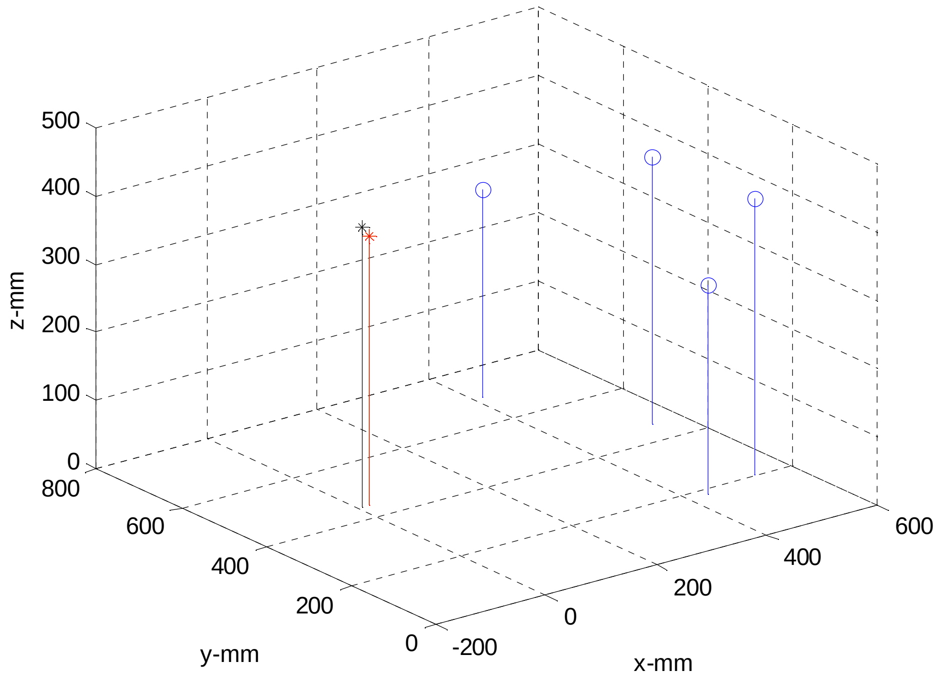

Figure 4.8, Positioning results using cross correlation method.

4.2.5 PD location using leading edge method with digital FIR filtering

An alternate way to fight AWGN noise is using a leading edge method with FIR (finite impulse response) digital filter. The bandwidth of the oscilloscope we used is 25MHz. However, the PD bandwidth ranges from 100 kHz to 300 kHz. If a bandpass or low-pass filter is used, the noise bandwidth will be dramatically reduced. A FIR filter is a generalized linear phased filter. This linear phase is critical to preserve the waveform of the original signals. For these reasons, a low-pass FIR digital filter was designed to filter out the noise outside of the signal bandwidth. We first Fourier transform the signal to find that the central frequency is at 150 kHz. The designed FIR filter is an equiripple filter with a pass band of 300 kHz and a stop band of 600 kHz. The pass band ripple is 1 dB and stop band is 60 dB below. Figure 4.9 shows the frequency response (amplitude and phase) of the designed FIR filter. The sampling frequency of the signals is f_s = 200MHz.

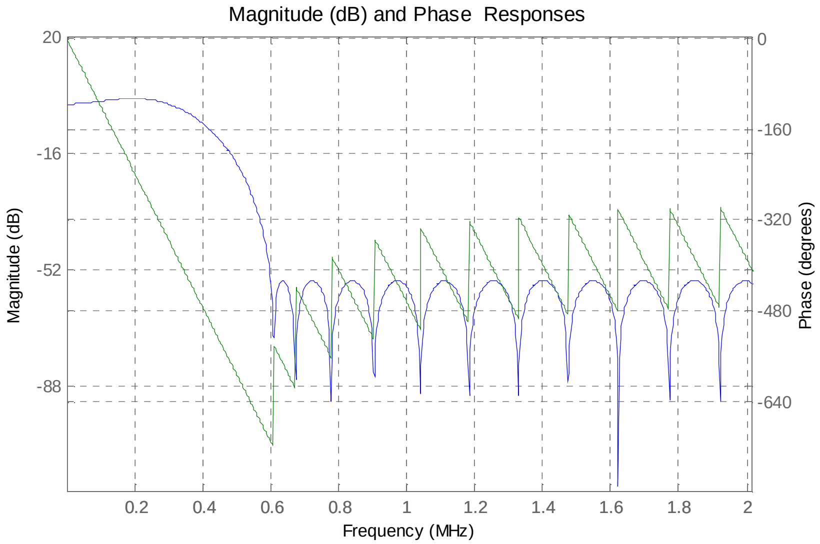

Figure 4.9 Frequency response of the FIR filter (green trace: phase response, blue trace: magnitude response).

Figure 4.10 shows the waveforms after the FIR filter. Compared with the waveforms in Figure 4.3, the AWGN noise components are dramatically reduced. Moreover, the peaks of the two signals have no half wave delay. The time difference of the two peaks is only 0.1 microseconds now. After we filtered the received signals, we can simply pick up the maximum absolute values of the waveforms and find the time delays. Figure 4.11 shows the positioning results with and without the FIR filter. We can see that the positioning results using FIR filter are more clustered than those without using the filter.

Table 4.1 lists the position localization results using the different methods. From this list, we can easily see that the location results using the cross-correlation method are more consistent than those using the other methods. The results using the leading edge with FIR filter have a pretty consistent result except the third set, which has reduced position errors. The position results using the convolution method have more errors than using both the cross-correlation and leading edge with FIR filter methods. The positioning results by directly picking the peaks of the waveform have more errors. Therefore we expect that using cross correlation and the leading edge method with FIR filter will lead to good positioning results. In section 4.3, we will give a statistical evaluation of the positioning using the three methods we mentioned above.

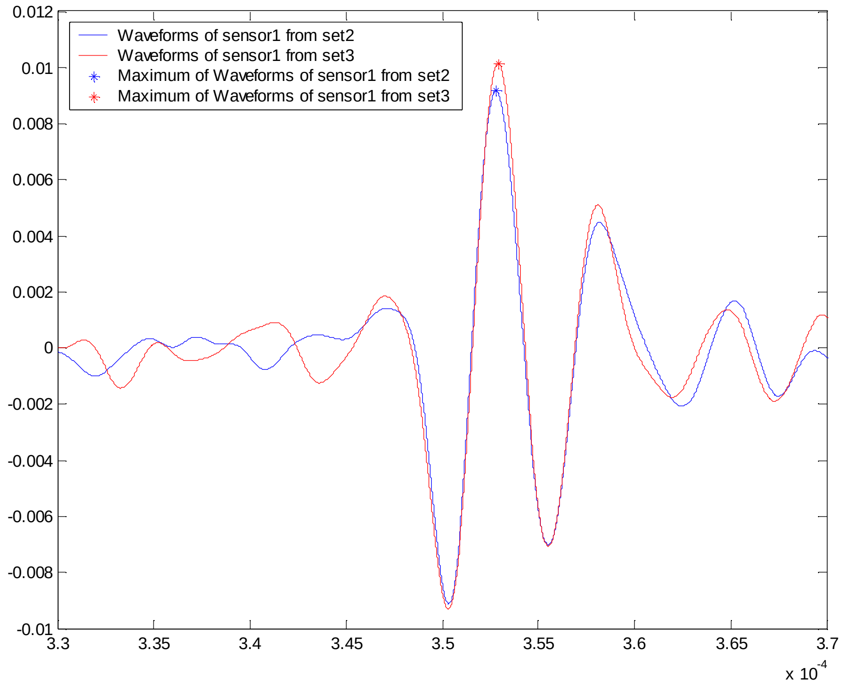

Figure 4.10, Two representative waveforms form sensor 1 after FIR filter

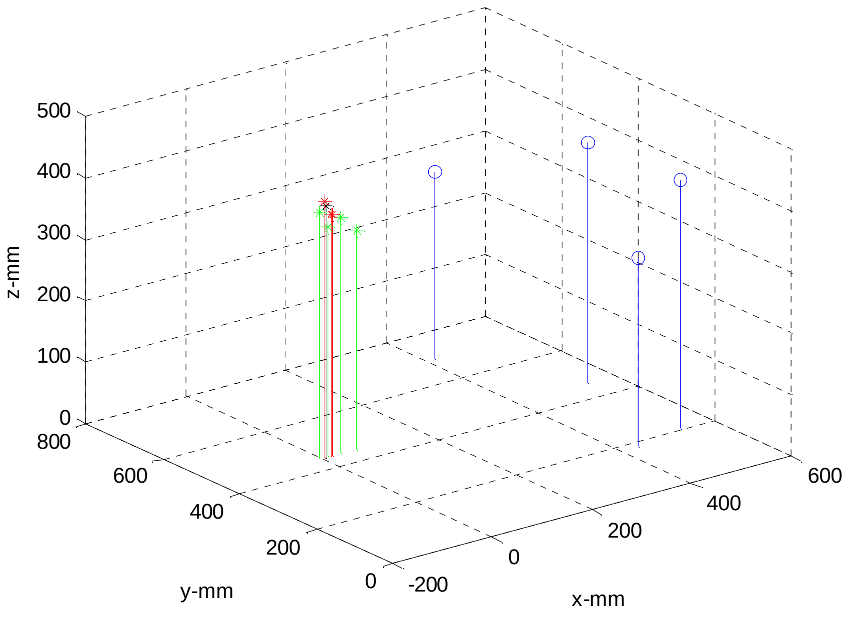

Figure 4.11, Positioning results using leading edge method with FIR filter (red) and without filter (green).

Table 4.1 Comparison of positioning results using different methods with the source located at (8.4, 446.1, 409.3). (The units are all in millimeters)

	Convolution	Cross correlation	FIR filter	Unfiltered
1	18.8, 446.0, 393.5	20.9, 446.0, 392.7	18.7, 446.0, 393.5	67.2, 442.6, 358.6
2	18.1, 446.0, 394.8	22.3, 446.0, 392.6	18.0, 446.0, 394.8	67.5, 442.4, 359.5
3	-35.4, 450.4, 433.3	23.0, 445.9, 392.4	7.3, 446.0, 416.3	42.7, 449.9, 382.4
4	20.8, 445.7, 392.6	21.1, 445.9, 393.4	20.6, 445.7, 392.8	-0.5, 450.1, 399.8
5	6.1, 449.8, 416.9	21.4, 445.9, 393.2	20.4, 445.6, 393.0	13.7, 446.0, 374.8

4.2.6 Relationship between positioning accuracy and sensor array layout

The PD position is calculated in x, y z coordinates. From Table 4.1, we find that the errors in the y direction are much smaller than those in the x or z direction. Inspecting the layout of the sensor array, we find that the spreading of the sensor array in three dimensions is 121.9mm in x direction, 511.4mm in y direction and 102.0mm in z direction. It is easy to determine that the greater the spreading in each axis, the less error. The positioning errors are related to the layout of the sensor arrays and the received signal to noise ratio. Therefore, the calculated positions will have different levels of errors in the x, y and z directions. In GPS, Dilution of Precision factors are used to account for the differences in positioning errors in different axes. Based on this fact, we would like to spread the sensor arrays in the transformer as much as possible. Placing one sensor on each corner of the transformer is the best configuration to spread the sensor arrays. This result coincides with the analysis in section 2.1.4, in which we spread the sensor arrays in order to gain the largest detection range.

4.3 Evaluation of the experimental results:

Three parameters can be used to evaluate the quality of the position results. They are accuracy, precision, and repeatability. When the acoustic source is not far away from the sensor arrays, SNR (signal to noise ratio) of the detected signal is high. This will give us a more accurate and highly repeatable position result. However, when the acoustic source is far away from the sensor array, the SNR is poor. Therefore we will expect that the position accuracy and repeatability will get worse.

Precision

How precisely we can locate the PD source is determined by the precision of the caliper, the parameters and the instrument we used in the experiment. The precision of the caliper we used to measure the coordinate system is 1 millimeter. The time precision of the oscilloscope is 1 microsecond. Considering 1 m/s sound wave precision in water, the distance measured by oscilloscope is 1 micron. So the system precision could potentially reach 1 millimeter.

Accuracy

How accurately we can locate a PD source is determined by the system precision, how errors are introduced during the measurement and the post data processing algorithms. In this system, the diameter of the PD source is 23 millimeters. The diameter of the sensor diaphragm is 2.5 millimeters. Also, there is an AWGN (additive white Gaussian noise) and multi-path interference, which introduce errors to the measurements. Also as mentioned in section 4.2.6, different sensor array layouts will result in different position errors in x, y and z directions. Unlike a GPS system, which is a digital communication system, this PD detection system is an analog system. Therefore, we cannot get any processing gain. These factors make it hard to estimate the system accuracy.

Repeatability

The repeatability of the positioning is mainly determined by the noise and interference sources, as well as what kind of algorithm is used for location. When the signal to noise ratio is poor, the deviation of average mean value will increase due to the noise interference.

This time we changed the layout between the sensor array and the acoustic source in the tank. Two sensors in the sensor array were farther away from the acoustic source. One sensor was moved to 810 millimeters away from the acoustic source and another one moved to 600 millimeters away from the acoustic source. The coordinate system is shown in Table 4.2. In order to get a statistical estimation of the quality of the positioning, we sampled the signal at each sensor 50 times. Based on our knowledge of stochastic signals, there will be 6,250,000 different combinations we can use to position the acoustic source. Although these combinations are not absolutely uncorrelated, we still can use them to give a statistical evaluation of the positioning. Next we are going to get the statistical positioning results using the three methods mentioned before.

Table 4.2 Coordinate system for the sensor and the PD source

	X(mm)	Y(mm)	Z(mm)
Sensor #1	411.6	194.9	307.6
Sensor #2	716.9	500.3	389.0
Sensor #3	358.7	714.3	354.0
Sensor #4	508.6	506.3	201.3
PD source	-33.4	417.1	411.1

4.3.1 Cross-correlation method

Due to limited computer speed, for the cross correlation method, 2500 different combinations were used to evaluate the statistical results of the positioning data. Figure 4.12 shows the position results. When we define an error cube with a side length of ±50 mm centered at the mean value of the positioned data, we find out the 94.48% of the data falls inside of the error cube. These 94.48% positioning results are shown as red stars in the figure. The rest of the positioning results which fall outside of this error cube are plotted as blue stars. Figure 4.13 shows the position data within a ±50 mm cube. It is easy to see that the positioning data are more concentrated in the range of 420mm to 430 mm on the y axis. The positioning data are more scattered in the x and z direction than in the y direction. These results can be confirmed from the histograms in each axis in Figure 4.14. Further inspection shows that these 94.48% positioning data are within a tolerance cube of $35.1 \times 9.8 \times 51.1$ mm^3, which is actually much smaller than the ±50 mm cube. These results indicate that we should spread the sensors as much as we can in order to increase the positioning accuracy. The total position data have a mean value of (-18.2, 423.5, 390.8) with standard deviations of (18.86, 3.13, 7.82). The total range of the data is within a $189.147\times26.7\times164.83$ mm^3 cube. The 94.48% position data has a mean of (-22.0, 424.2, 391.5) with standard deviations of (9.15, 1.59, 6.44).

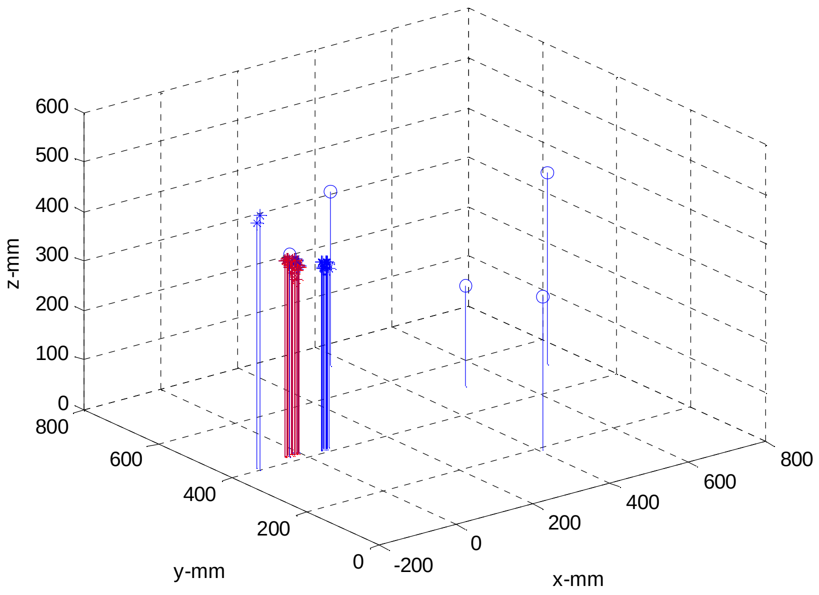

Figure 4.12, Positioning results using the cross-correlation method (red star, within ±50 mm cube, blue star, outside of ±50 mm cube).

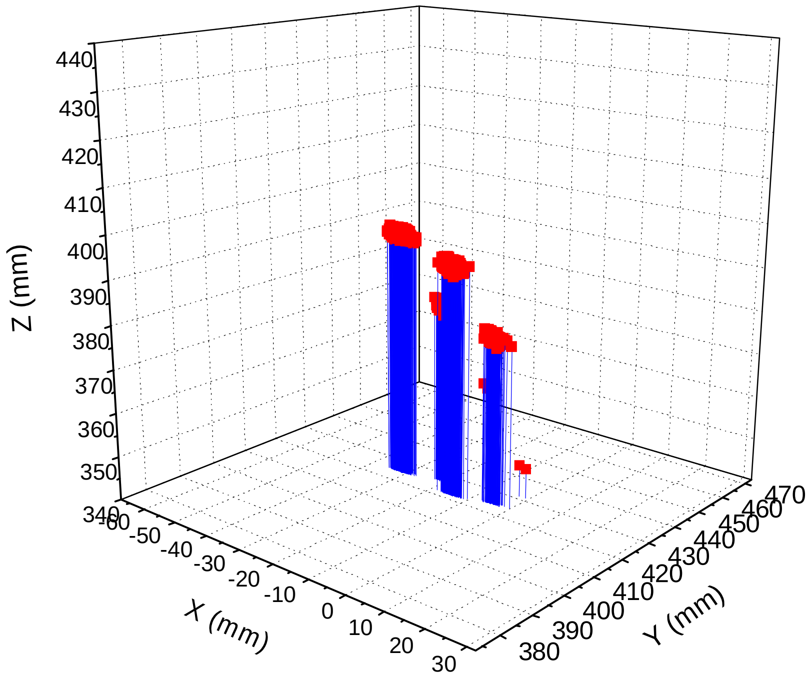

Figure 4.13, Position data (red square) within the ±50 mm cube.

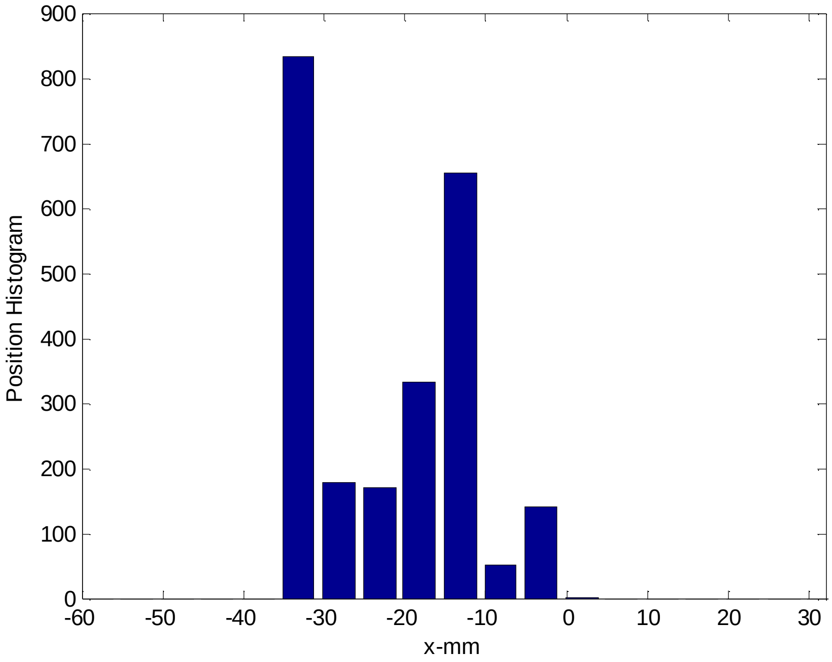

Figure 4.14 (a)

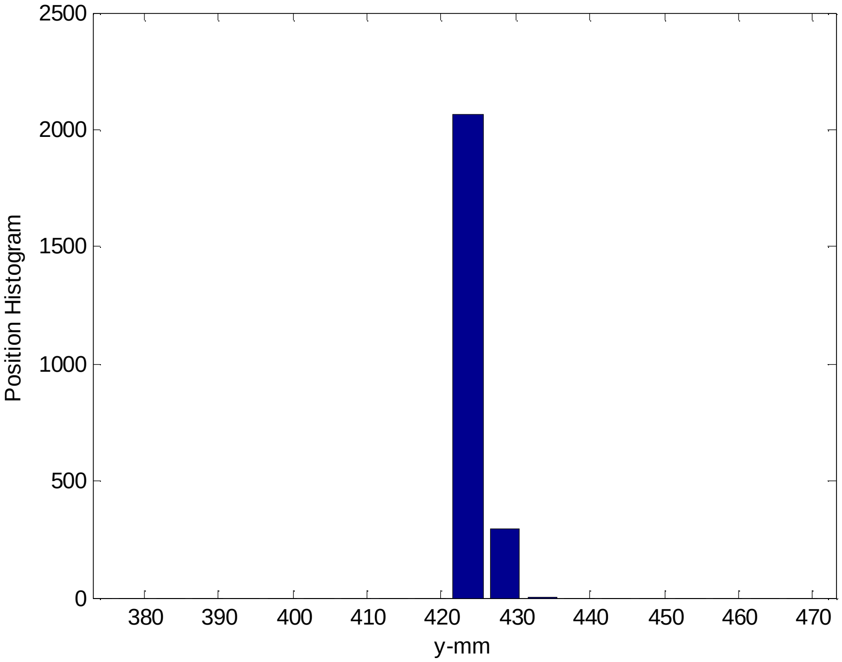

Figure 4.14 (b)

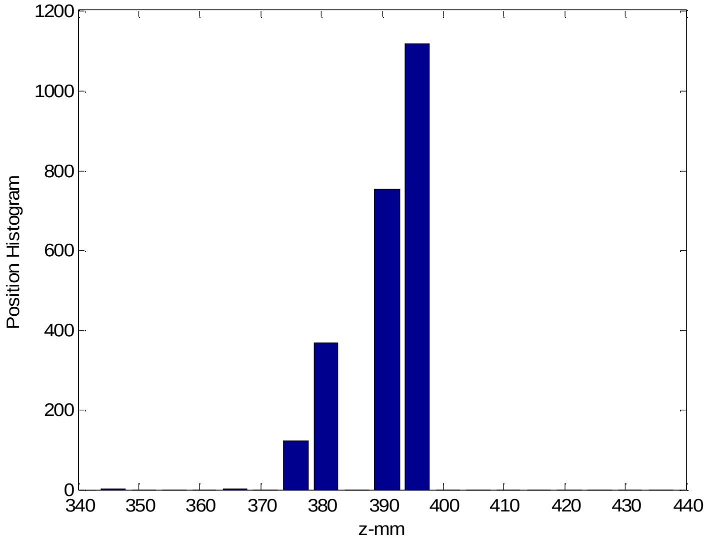

Figure 4.14(c)

Figure 4.14, Histograms of the positioned data on the x (a), y (b) and z (c) axes using the cross-correlation method.

4.3.2 Leading edge method with FIR filter

This time, we also take 2500 different combinations to evaluate the statistical results of the positioning using the FIR filter method. Figure 4.15 shows the position results. When we define an error cube with a side length of ±50 mm centered at the mean value of the positioned data, we find that 100% of the data falls inside of the error cube. All positioning results are shown as red stars. Figure 4.16 shows the position data within the ±50 mm cube. The positioning data are more concentrated around the real PD source than those results by using the cross-correlation method. Figure 4.17 shows the histograms in each axis. It is easy to see that the positioning data are more concentrated in the range of 420mm to 430 mm on the y axis. The positioning data in the x direction are more scattered than on the y axis. Further inspection shows that all the positioning data are within a tolerance cube of 22.7×4.1×5.3 mm^3, which is smaller than the results of the 94.48% positioning data using cross-correlation method. . The total position data have a mean value of (-17.5, 422.8, 392.8) with standard deviations in each axis of (6.08, 0.99, 1.42). These results show that the leading edge method with the FIR filter results in better position location performance.

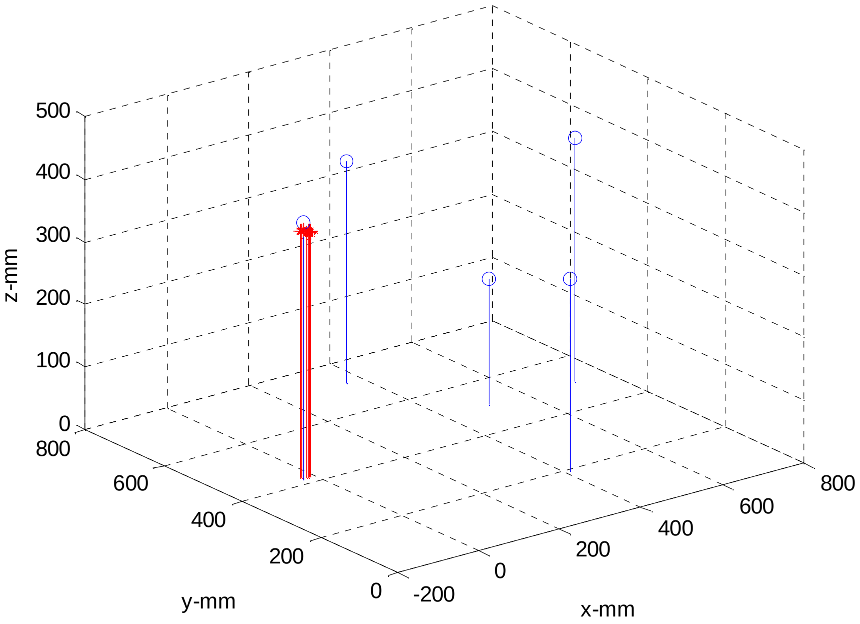

Figure 4.15, Position location results (red star) using FIR filter method.

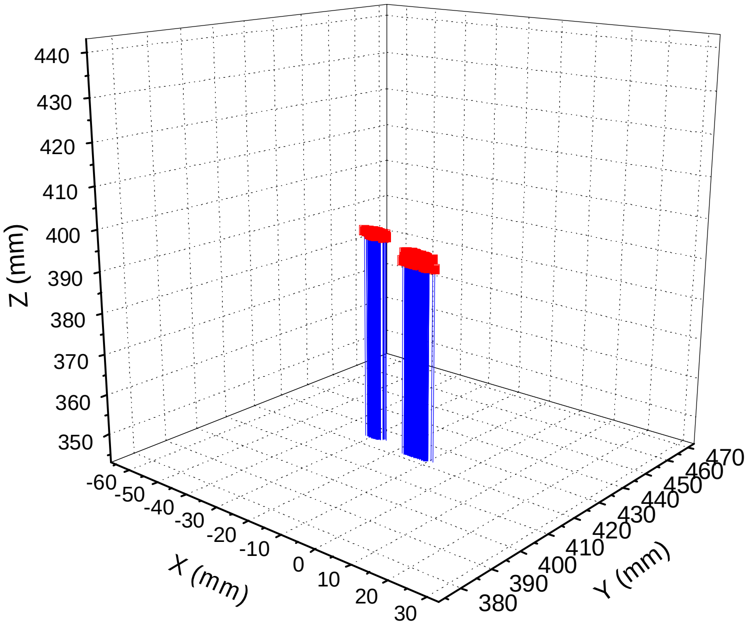

Figure 4.16, Positioning results (red square) within the ±50 mm cube.

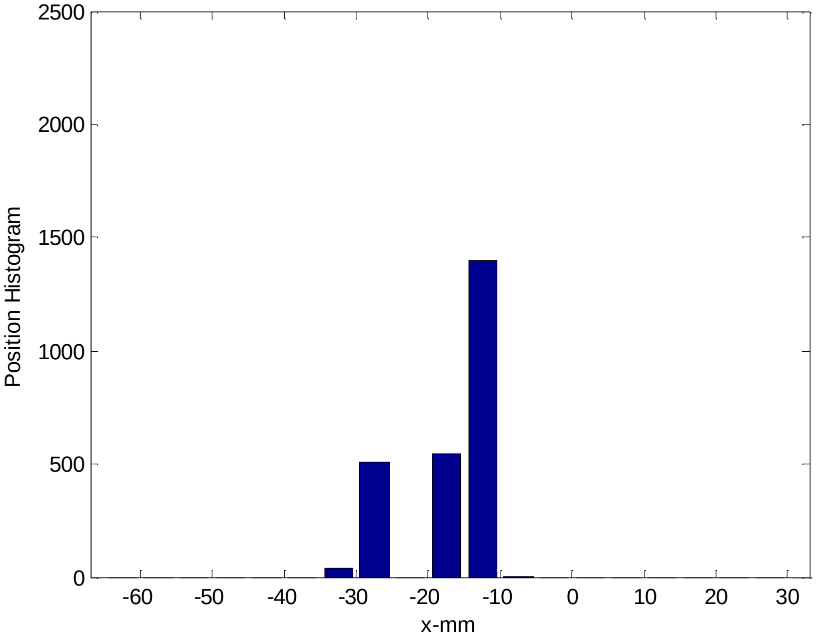

Figure 4.17 (a)

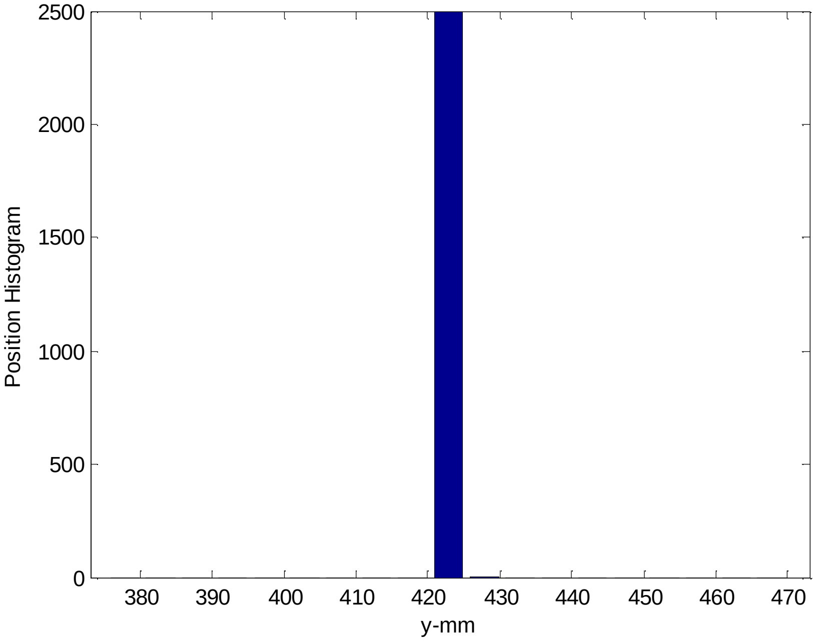

Figure 4.17(b)

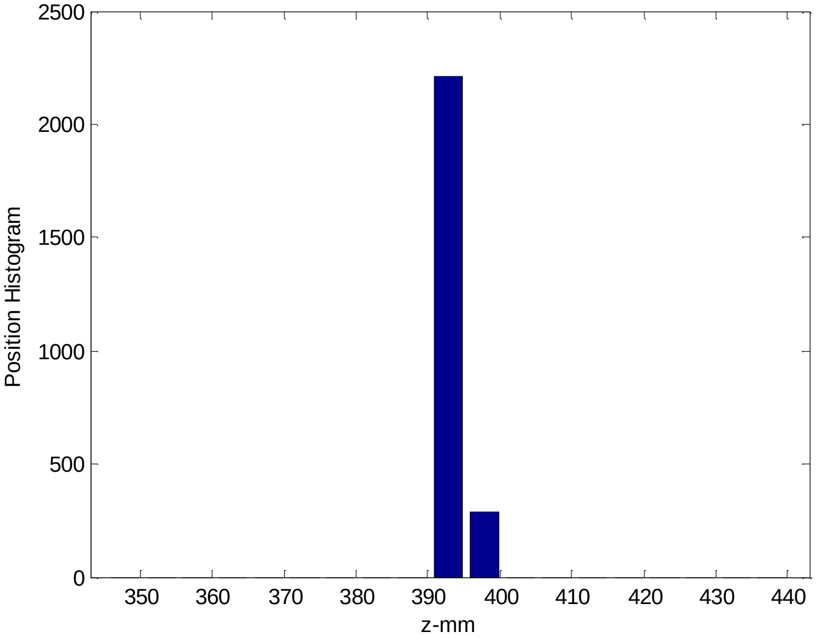

Figure 4.17 (c)

Figure 4.17, Histograms of the positioning data on the x (a), y (b) and z (c) axes using the leading edge method with FIR filter.

4.3.3 Convolution method

Because of the higher calculation burden of the convolution method, 787 different combinations were used for evaluation. The results show that 81.7% of the position results fall inside of the 100×100×100 mm^3 error tolerance cube. Figure 4.18 shows the positioning data within the error cube (red star) and outside of the error cube (blue star). Figure 4.19 shows the position data within the ±50 mm cube. Figure 4.20 shows the histogram of data within this ±50 mm cube. The positioning data are more scattered than those using the cross-correlation and the leading edge method with FIR filter. Also we find that the data are more concentrated on the y axis than on the x and z axes due to the sensor array layout. Further inspection shows that these 81.7% positioning data are within a tolerance cube of 85.9×21.1×52.7 mm^3 cube, which is actually much smaller than the ±50 mm cube.

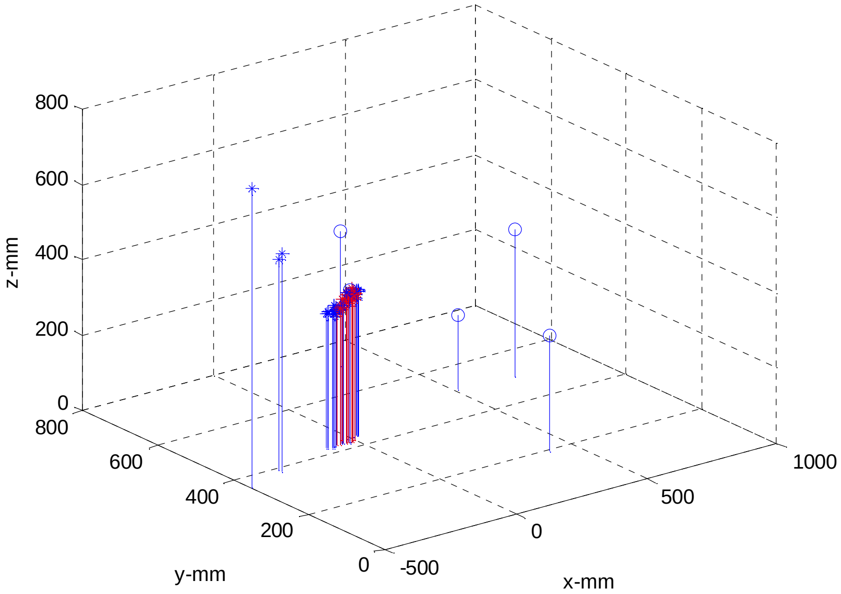

Figure 4.18, Positioning result using convolution method (red star, within ±50 mm cube, blue star, outside of ±50 mm cube)

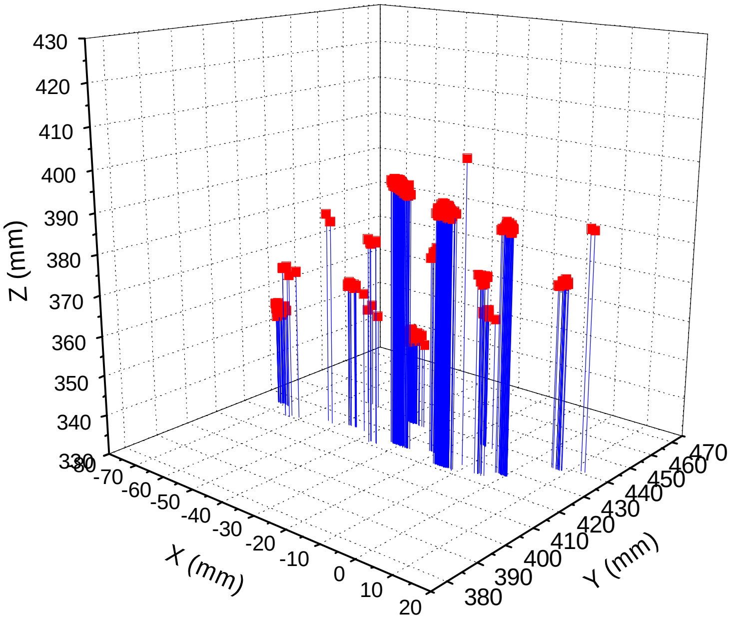

Figure 4.19, Distribution of the positioning results within the ±50 mm error cube.

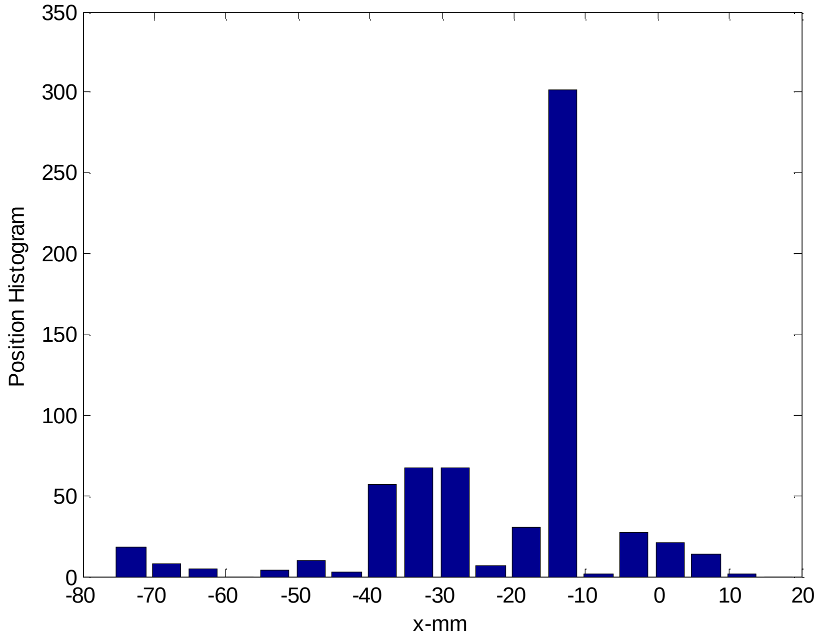

Figure 4.20(a)

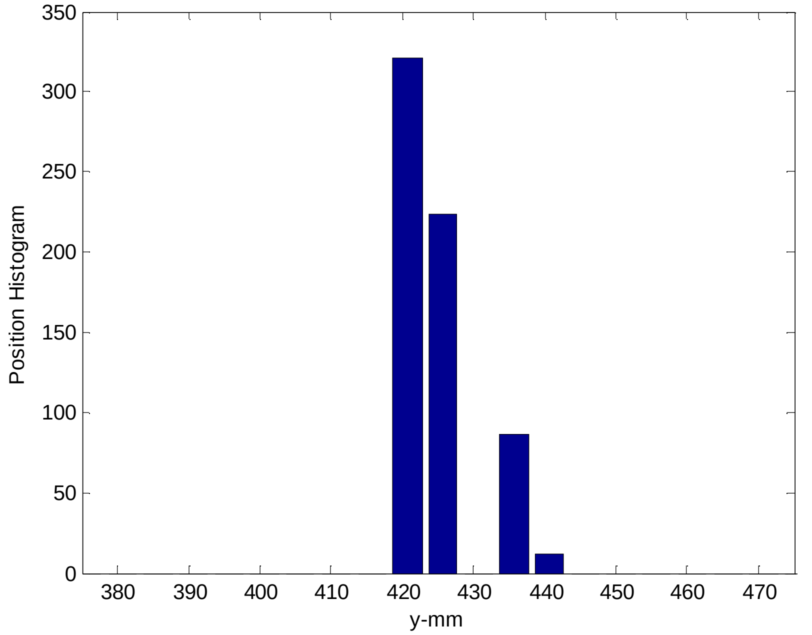

Figure 4.20(b)

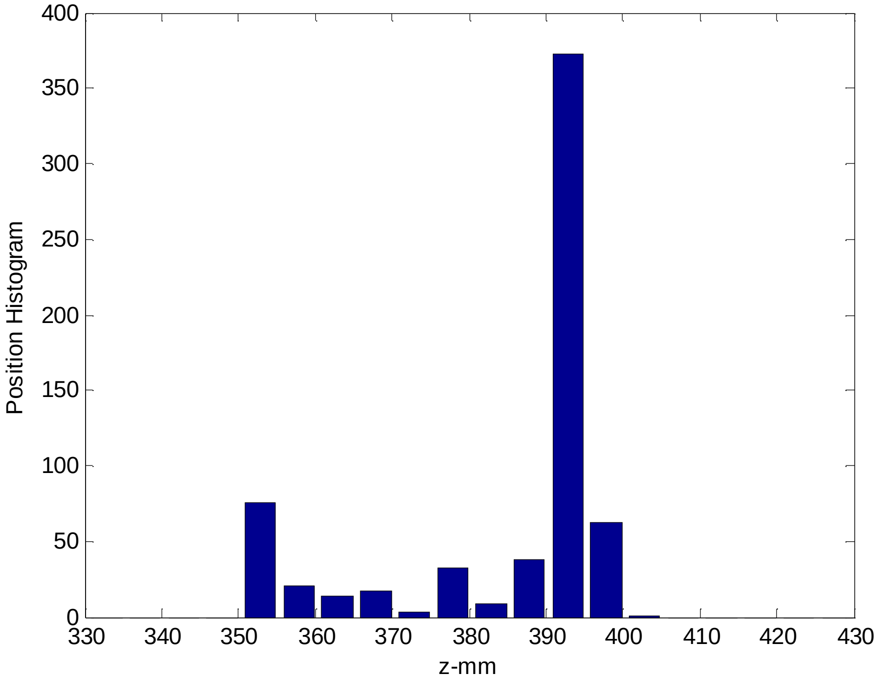

Figure 4.20(c)

Figure 4.20, Histogram of the positioning data in x (a), y (b) and z (c) axes using the convolution method.

4.3.4 Discussion

Inspecting Figures 4.13, 4.16 and 4.19, we find that the positioning data concentrate in several clusters. Two reasons account for these results. One is that the 2500 (for the cross-convolution and the leading edge method with the FIR filter) or 787(for the convolution method) combination of data are correlated. The actual data are sampled at each sensor 50 times. We then recombine the data to localize the PD positions. A second reason is that during the measurement, the received signal changes phases because we have to adjust the Q-point tuning system to get the maximum SNR. These phase changes cause the positioned data clustered. In order to get the real statistical results, we need to use random sampled data to analyze. Figure 4.14, 4.17 and 4.20 show the histograms of the positioning data in 20 bins for each axis for different methods. From the histogram of each axis, we can find that the value of each bin varies a lot. That means that there exists one positional value that has a high probability. In a real power transformer, when there is a PD activity, the PD activity will likely repeat again. This repeatable activity can help to fight the positioning errors. The greater number of times we detect the PD signals, the more accurately we can locate the PD site. The expected position of the PD sources are (-22.0, 424.2, 391.5) with standard deviations of (9.15, 1.59, 6.44) for the cross-correlation method, (-17.5, 422.8, 392.8) with standard deviations of (6.08, 0.99, 1.42) for the leading edge method with FIR filter method, and (-23.0, 425.7, 384.7) with standard deviations of (15.83, 5.44, 14.44) for the convolution method. These expected positioning results are different from the PD position measured as (-33.4, 417.1, 411.1) in Table 2. These errors are mainly caused by measurement errors in the coordinate systems. Any small measurement errors in the sensor coordinate system will introduce large errors in the final location calculation using the TDOA method. The large standard deviation in the x and z axes are mainly introduced by the layout of the sensors. An improved sensor array layout would spread the sensors as much as possible. In order to reduce the total deviation in each axis, we need to increase the signal to noise ratio of the received signal. For the current experiment, we can either increase the intensity of the acoustic source or increase the sensor's sensitivity. In a real system, we would like the system to be capable of detecting weak PDs; therefore, increasing the sensor's sensitivity should be considered in future work. From equation (2.1) in Chapter 2, we find that the sensitivity of the sensor is proportional to the radius of the diaphragm (a^3) and inversely proportional to the thickness of the diaphragm (h^3). Therefore we can either increase the radius or decrease the thickness of the diaphragm. However, simply changing either the radius or the thickness of the diaphragm will change the natural frequency of the sensor, which, if changed too much, may fall out of the frequency range of partial discharges. Inspecting equation 2.2 in Chapter 2, we find that the natural frequency of the sensor is proportional to h and inversely proportional to a^2. One way to increase the sensor's sensitivity while keeping the natural frequency unchanged is to increase the thickness of the diaphragm, and at the same time, increase the radius of the diaphragm to keep the ratio of the a^2/h unchanged.

References:

1. Y. T. Chan, K. C. Ho, A simple and efficient estimator for hyperbolic location, IEEE Transaction on signal processing, vol. 42, no. 8, pp1905-1915, 1994.
2. Alison K. Lazarevich, “Partial Discharge Detection and Localization in High Voltage Transformers Using an Optical Acoustic Sensor”, Virginia Tech Masters Thesis, May 2003.

Chapter 5 Summary and Future Work

5.1 Summary of the work

In this thesis work, the requirements for a fiber sensor suitable for detecting partial discharges in transformers are discussed. An EFPI sensor design is detailed. These include the sensor structure, operating principle, sensitivity and frequency response.

Two dimensional and three dimensional ANSYS models of the fiber sensor were built for this project. By using static, modal and harmonic analysis functions in ANSYS 7.0, we obtained the deformation, modal solution and frequency response of the sensor. The angular dependence of the frequency response was also modeled using Finite Element Methods. Sensor frequency response testing was tested in a 500 gallon water tank. The results show that the sensor's frequency response is between 100 kHz and 300 kHz. The angular dependence of the frequency response was tested and analyzed. Results show that the sensor's response drops 3-5 dB around 30 to 45 degrees. This information is helpful for the design of the complete sensor system.

Location of a partial discharge was demonstrated in a 500 gallon water tank. Three methods, cross-correlation, leading edge with digital FIR filter and convolution, were used to precisely determine the TDOA (time difference of arrivals). The cross-correlation method and the leading edge method with digital FIR filter were confirmed to be more robust than the convolution method. Finally it is demonstrated that 94.48% of the position data are bounded by a $35.1\times9.8\times51.1$ mm^3 cube using the cross-correlation method, and 100% of the position data are bounded by a $22.7\times4.1\times5.3$ mm^3 cube using leading edge method with FIR filter, with a sensing range of 810 mm in a 500 gallon water tank.

The objective of this thesis is to determine the optimal sensor array layout which can monitor the whole transformer and also provide the best localization results. From the monitoring scope of the sensor, sensor's sensitivity, angular dependence of the frequency response of the sensor and the position location results, it is found that we need to spread the sensors to each corner of the transformer. However, when the sensor's sensitivity is limited, we can divide the transformer into several small cubes. This way we can monitor the whole unit, but the tradeoff is that we need more sensors.

5.2 Future work

In order to make the PD detection and location system practical for a real transformer, further development is necessary. The first thing is to increase the dynamic range of the sensor's sensitivity. From the experimental results on PD location, we find that a poor signal to noise ratio is the main cause of position errors. Because the AWGN noise of the detector is constant, the only way to increase the signal to noise ratio is to increase the sensor's sensitivity. This was discussed in section 4.3.4.

The second work is to increase the stability of the sensor. The current sensor is still not stable when operated in water. This instability will reduce the signal to noise ratio, thus affect the PD positioning. The sensor may even fail to detect a PD event. Also, this instability will introduce a phase shift, which will affect the accuracy of the positioning results

Multipath interference is a problem in the real system when there is vibration. These fading channels not only alter the properties of PD waveforms, but also introduce random fluctuations to the amplitude and phase of the PD signals. Measures have to be taken to reduce this multipath interference. Sound absorption material can be used on the transformer tank to absorb reflections. A theoretical model and a simulation can be built and efforts should be made to find if there is any post processing method to overcome the effect of multipath interference.

More sensors should be used in the tank simultaneously either by multiplexing or using multiple optical sources. Also, as demonstrated before, the sensor array layout can affect the positioning accuracy. The greater the spread of the sensor layout, the more accurate the positioning results. However, because of the limitation of the sensor's sensitivity, the experimental layout as shown in Figure 2.1 was not demonstrated. From the current experimental results, we believe that an error tolerance cube of $5\times5\times5$ mm^3 can be easily achieved when a higher sensitivity sensor is available.

Finally, before the system can be used in real transformers for PD detection and position location, an evaluation of the accuracy, precision and the system repeatability should be quantified. We demonstrated that 100% positioning data fell in a $22.7\times4.1\times5.3$ mm^3 error cube with a sensing range of 810mm. An accuracy of ±10 millimeters on each axis and a repeatability of above 99% should be reached for a 2 meter range. In order to achieve this result, a high sensitivity sensor and an improved signal processing system are desired. Although PD events occur randomly, when there is one PD, it is likely to have more PD activities in the future. So a system that can store and process the information of previous PD events can help identify the real PD location and can be used to minimize the location errors.

Appendix1, Program for Angular Frequency Response in ANSYS 7.0 :

```
!!!!!!!!!!!!!!!!!!!!!!!!!!!!!!!!!!!!!!!!!!!!!!!!!!!!!!!!!!!!!!!!!!!!!!!!!!!!!!!!!!!!!!!!!!!!!!!!!!!!!!!!!!!!!!!!!!!!!!!!!!!!!!!!!!!!!!!!!!!!!!!!!!!!!!!!!!!!!!!!!!!!!!!!!!!!!!!!!!!!!!!!!!!!!!!
/COM,-------------- 3 dimensional model of frequency response simulation of a fiber sensor
/COM,-------------- Oct. 2004. Lijun Song @ Virginia Tech
!!!!!!!!!!!!!!!!!!!!!!!!!!!!!!!!!!!!!!!!!!!!!!!!!!!!!!!!!!!!!!!!!!!!!!!!!!!!!!!!!!!!!!!!!!!!!!!!!!!!!!!!!!!!!!!!!!!!!!!!!!!!!!!!!!!!!!!!!!!!!!!!!!!!!!!!!!!!!!!!!!!!!!!!!!!!!!!!!!!!!!!!!!!!!!!
/CLEAR,START
/COM,ANSYS RELEASE  7.0    UP20021010       21:28:58    10/14/2004
!*
/TITLE, 3D acoustic analysis of a fiber sensor
*SET,diaH , 0.15E-3             ! Thickness of the diaphragm
*SET,diaR , 1.25E-3             ! Radius of the diaphragm
*SET,supH , 0                   ! Thickness of the supporting tube
*SET,tubL ,1E-3                 ! Length of supporting tube
*SET,c,1480                     !acoustic speed
*SET,freqSource,100e3           !frequency of source, wavelength=c/freqSource
*SET,lamda,c/freqSource         !wavelength of the longest wave
/VIEW,1,-1,-2,2                 ! Change viewpoint
/PREP7                          ! Enter preprocessor

!!!!!!!!!!!!!!!!!!!!!!!!!!!!!!!!!!!!!!!!!!!!!!!!!!!!!!!!!!!!!!!!!!!!!!!!!!!!!!!!
/COM,-------------- Element and real constant tables
!!!!!!!!!!!!!!!!!!!!!!!!!!!!!!!!!!!!!!!!!!!!!!!!!!!!!!!!!!!!!!!!!!!!!!!!!!!!!!!!
ET,1, SHELL63                   ! 4-node shell with U and ROT DOFs for membrane
ET,2,FLUID30                    ! 8-node solid with UX,UY,UZ, PRES DOFs
                                ! interface elements/structure present
ET,3,FLUID30,,1                 ! 8-node fluid element with PRES DOFs for air/structure absent
ET,4,SHELL63                    ! acoustic element
R,1,DiaH                        !Thickness of diaphragm
R,2,0                           !Reference pressure
R,3,0
R,4,diaH

!!!!!!!!!!!!!!!!!!!!!!!!!!!!!!!!!!!!!!!!!!!!!!!!!!!!!!!!!!!!!!!!!!!!!!!!!!!!!!!!
/COM,-------------- Material property tables
!!!!!!!!!!!!!!!!!!!!!!!!!!!!!!!!!!!!!!!!!!!!!!!!!!!!!!!!!!!!!!!!!!!!!!!!!!!!!!!!
MP,EX,1,3.65E10                 ! Young's modulus of diaphragm  "E"
MP,NUXY,1,0.17                  ! Poisson's ratio  "     "     "  "        "Nu"
MP,DENS,1,1100.5                ! Density
MP,DENS,2,1000
MP,SONC,2,1480
MP,DENS,3,1000
MP,SONC,3,1480
MP,MU,3,1
MP,EX,4,3.65E10                 ! Young's modulus of diaphragm  "E"
MP,NUXY,4,0.17                  ! Poisson's ratio  "     "     "  "        "Nu"
MP,DENS,4,1100.5                ! Density

!!!!!!!!!!!!!!!!!!!!!!!!!!!!!!!!!!!!!!!!!!!!!!!!!!!!!!!!!!!!!!!!!!!!!!!!!!!!!!!!
!!/COM,-------------- Build 3D model and MESH
!!!!!!!!!!!!!!!!!!!!!!!!!!!!!!!!!!!!!!!!!!!!!!!!!!!!!!!!!!!!!!!!!!!!!!!!!!!!!!!!
CSYS,0                          ! Activates coordinate system. (cylinder)
CYLIND,0,DIAR,0,-TUBL
CYLIND,0,DIAR,-TUBL,-LAMDA
CYLIND,0,DIAR,0,LAMDA
CYLIND,DIAR,LAMDA,0,-TUBL
```

```
CYLIND,DIAR,LAMDA,-TUBL,-LAMDA
CYLIND,DIAR,LAMDA,0,LAMDA
/REPLOT
NUMMRG,KP
ASEL,S,AREA,,1,4,1,0
APLOT
AATT,1,1,1
AMESH,1
AMESH,2
AMESH, 3
AMESH,4
ALLS
VSEL,S,VOLU,,2,6,1
VATT,2,3,3
VSWEEP,2
VSWEEP,3
VSWEEP,4
VSWEEP,5
VSWEEP,6

!!!!!!!!!!!!!!!!!!!!!!!!!!!!!!!!!!!!!!!!!!!!!!!!!!!!!!!!!!
!!/COM,-------------- Change fluid attached to the structure as fluid 30 structure present
!!                    Element type 2, real number 2 and material property 2
!!                    APPLY FSI
!!!!!!!!!!!!!!!!!!!!!!!!!!!!!!!!!!!!!!!!!!!!!!!!!!!!!!!!!!
ESEL,S,TYPE,,1
EPLOT
/PNUM,KP,0
/PNUM,LINE,0
/PNUM,AREA,0
/PNUM,VOLU,0
/PNUM,NODE,0
/PNUM,TABN,0
/PNUM,SVAL,0
/NUMBER,0
!*
/PNUM,TYPE,1
/REPLOT
!*
NSLE,S
NPLOT
elist,all,,,1,0
ESLN,S
elist,all,,,1,0
ESEL,R,TYPE,,3
elist,all,,,1,0
EPLOT
MAT,2
REAL,2
TYPE,2
EMODIF,ALL
/REPLOT
ALLS

!!!!!!!!!!!!!!!!!!!!!!!!!!!!!!!!!!!!!!!!!!!!!!!!!!!!!!!!!!
!!/COM,-------------- Change fluid outside to absorptive element
```

```
!!                         Element type 3, real number 3 and material property 3
!!/COM,-------------- DEFINE Impedance Surface (IMPD)
!!!!!!!!!!!!!!!!!!!!!!!!!!!!!!!!!!!!!!!!!!!!!!!!!!!!!!!!
CSYS,1
NSEL,S,LOC,Z,LAMDA
NPLOT
NSEL,A,LOC,Z,-LAMDA
NPLOT
NSEL,A,LOC,X,LAMDA
/REPLOT
ESLN,S
MAT,3
REAL,3
TYPE,3
EMODIF,ALL
ALLS
alist, all

!!!!!!!!!!!!!!!!!!!!!!!!!!!!!!!!!!!!!!!!!!!!!!!!!!!
!---------------------------Duplicate shell 63 element and coupling the nodes
!!!!!!!!!!!!!!!!!!!!!!!!!!!!!!!!!!!!!!!!!!!!!!!!!!
!!!!AGEN, ITIME, NA1, NA2, NINC, DX, DY, DZ, KINC, NOELEM, IMOVE:
AGEN,2,1,4,1,,,,0,0,
ASEL,S,AREA,,6
ASEL,A,AREA,,9
ASEL,A,AREA,,17
ASEL,A,AREA,,18
APLOT
ESLA,
MAT,1
REAL,4
TYPE,4
EMODIF,ALL
EPLOT
ALLS
ESEL,S,TYPE,,1
ESEL,A,TYPE,,4
NSLE
CPINTF,UX,1e-8
CPINTF,UY, 1e-8
CPINTF,UZ, 1e-8
CPINTF,ROTX, 1e-8
CPINTF,ROTY, 1e-8
CPINTF,ROTZ,1e-8
ALLS
FINISH

!!!!!!!!!!!!!!!!!!!!!!!!!!!!!!!!!!!!!!!!!!!!!!!!!!!!!!!!
!!/COM,-------------- APPLY FSI
!!!!!!!!!!!!!!!!!!!!!!!!!!!!!!!!!!!!!!!!!!!!!!!!!!!!!!!!
/PREP7
FSST
ESEL,S,TYPE,,1
EPLOT
NSLE
NPLOT
```

```
ESLN
EPLOT
ESEL,S,TYPE,,2
EPLOT
ELIST
NLIST
NPLOT
FLST,5,20186,2,ORDE,2
FITEM,5,1
FITEM,5,-20186
CM,_Y,ELEM
ESEL, , , ,P51X
CM,_Y1,ELEM
CMSEL,S,_Y
CMDELE,_Y
!*
/GO
SFE,P51X,1,FSIN, ,1,
ESEL,S,TYPE,,1
NSLE
ESLN
ESEL,R,TYPE,,2
SF,ALL,FSI
ALLS

!!!!!!!!!!!!!!!!!!!!!!!!!!!!!!!!!!!!!!!!!!!!!!!!!!!!!!!!!!!!!!!!!!!!
!!/COM,-------------- DEFINE Impedance Surface (IMPD)
!!!!!!!!!!!!!!!!!!!!!!!!!!!!!!!!!!!!!!!!!!!!!!!!!!!!!!!!!!!
CSYS,1
NSEL,S,LOC,Z,LAMDA
NSEL,A,LOC,Z,-LAMDA
NSEL,A,LOC,X,LAMDA
ESLN
SF,ALL,IMPD,1
ALLS

!!!!!!!!!!!!!!!!!!!!!!!!!!!!!!!!!!!!!!!!!!!!!!!!!!!!!!!!!!!
!!/COM,-------------- DEFINE Boundary conditions
!!!!!!!!!!!!!!!!!!!!!!!!!!!!!!!!!!!!!!!!!!!!!!!!!!!!!!!!!!!
csys,1
ESEL,S,TYPE,,1
NSLE,S
NSEL,R,LOC,X,DIAR
D,ALL, ,0, , , ,UX,UY,UZ,ROTX,ROTY,ROTZ
ALLS
ESEL,S,TYPE,,1
NSLE,S
NSEL,R,LOC,Z,-TUBL
D,ALL, ,0, , , ,UX,UY,UZ,ROTX,ROTY,ROTZ
ALLS
FINISH

!!!!!!!!!!!!!!!!!!!!!!!!!!!!!!!!!!!!!!!!!!!!!!!!!!!!!!!!!!!
!!/COM,-------------- SOLVE
!!!!!!!!!!!!!!!!!!!!!!!!!!!!!!!!!!!!!!!!!!!!!!!!!!!!!!!!!!!
```

```
/SOLU
!*
ANTYPE,2
MSAVE,0
!*
MODOPT,UNSYM,5
EQSLV,FRONT
MXPAND,5, , ,0
LUMPM,0
PSTRES,0
!*
MODOPT,UNSYM,5,100000,300000, ,OFF
/STATUS,SOLU
SOLVE
FINISH
/POST1
SET,LIST,2
SET,LIST
SET,FIRST
SET,LIST
FINISH


/SOL
!*
ANTYPE,3
ESEL,S,TYPE,,1
EPLOT
FLST,2,1,5,ORDE,1
FITEM,2,2
/GO
!*
SFA,P51X,1,PRES,10000
HARFRQ,100000,300000,
NSUBST,30,
KBC,1
!*
ALLS
HARFRQ,100000,300000,
NSUBST,20,
KBC,1
!*
/STATUS,SOLU
SOLVE
FINISH
```

Appendix 2, Matlab Script for Position Location

1. Main code

```
%%%%%%%%%%%%%%%%%%%%%%%%%%%%%%%%%%%%%%%%%%%
%      Matlab script for hyperbolic position fixing. Four of the five      %
%      sensors are used to estimate the source location.                   %
%      Jan. 2004. Lijun Song @ Virginia Tech                               %
%%%%%%%%%%%%%%%%%%%%%%%%%%%%%%%%%%%%%%%%%%%

clear all
close all
%%%%%%%%%%%%%%%%%%%%%%%%%%%%%%%%%%%%%%%%
%PART1, measure the distance of each sensor and acoustic source to  %
%the O, X, Y points. 15 measurements are taken for each point with 5 %
%measurements taken in for each O X Y per point. The values of each %
%point is calculated by standard average of the 5 sample values.       %
%%%%%%%%%%%%%%%%%%%%%%%%%%%%%%%%%%%%%%%%

XY=[630.9 630.9 631.0 630.8 630.4];
OY=[522.2 522.2 522.6 523.0 523.0];
OX=[305.1 305.0 305.1 305.0 304.9];
xy=sum(XY)/length(XY);
oy=sum(OY)/length(OY);
ox=sum(OX)/length(OX);
%
sensor1O=[549.5 549.2 549.9 549.7];
sensor1X=[379.9 379.6 379.0 379.2 ];
sensor1Y=[644.3 644.4 644.8 643.9 645.0];
%
sensor2O=[957.9 956.9 955.6 956.8 957.0];
sensor2X=[755.2 756.0 756.4 755.5 755.9];
sensor2Y=[861.9 862.1 862.0 861.9 862.0];
%
sensor3O=[845.7 845.2 845.1 845.2 845.1];
sensor3X=[765.1 765.4 765.7 765.1 765.8];
sensor3Y=[610.6 610.1 610.5 610.5 610.4 ];
%
sensor4O=[873.9 873.9 874.1 873.9 875.1];
sensor4X=[798.9 798.8 799.1 799.1 799.2 ];
sensor4Y=[575.9 576.0 576.4 575.8 575.9];
%
sensor5O=[744.2 746.5 745.1 745.5 745.3];
sensor5X=[581.9 581.9 581.6 581.6 581.0];
sensor5Y=[595.3 596.1 595.1 596.7 596.2];
%
sourceO= [586.8 586.0 586.0 587.0 587.1];
sourceX= [676.7 676.4 676.2 676.0 676.5];
sourceY= [424.0 423.5 424.5 424.8 424.4];

measures=zeros(5,3);
```

```
measures(1,1)=sum(sensor1O)/length(sensor1O);
measures(1,2)=sum(sensor1X)/length(sensor1X);
measures(1,3)=sum(sensor1Y)/length(sensor1Y);

measures(2,1)=sum(sensor2O)/length(sensor2O);
measures(2,2)=sum(sensor2X)/length(sensor2X);
measures(2,3)=sum(sensor2Y)/length(sensor2Y);

measures(3,1)=sum(sensor3O)/length(sensor3O);
measures(3,2)=sum(sensor3X)/length(sensor3X);
measures(3,3)=sum(sensor3Y)/length(sensor3Y);

measures(4,1)=sum(sensor4O)/length(sensor4O);
measures(4,2)=sum(sensor4X)/length(sensor4X);
measures(4,3)=sum(sensor4Y)/length(sensor4Y);

measures(5,1)=sum(sensor5O)/length(sensor5O);
measures(5,2)=sum(sensor5X)/length(sensor5X);
measures(5,3)=sum(sensor5Y)/length(sensor5Y);

Asource=zeros(1,3);
Asource(1,:)=sum(sourceO)/length(sourceO);Asource(1,2)=sum(sourceX)/length(sourceX);Asou
rce(1,3)=sum(sourceY)/length(sourceY);

%%%%%%%%%%%%%%%%%%%%%%%%%%%%%%%%%%%%%%%%
%PART II, find the coordinate values of four sensors and the acoustic        %
% source from the values given above by calling function coordinate.          %
% Coordinate values for each sensor are saved in matrix of measures.          %
% Coordinate values for acoustic source are saved in Asources                 %
%%%%%%%%%%%%%%%%%%%%%%%%%%%%%%%%%%%%%%%%
numOfSensors=5;
sensorLocation=zeros(numOfSensors,3);
sensors=zeros(4,3);

for m=1:numOfSensors             %coordinates of sensors
   sensorLocation(m,:)=coordinate(measures(m,:), ox, oy, xy);
   Kall(m)=sum(sensorLocation(m,:).^2);
end
source=coordinate(Asource, ox, oy, xy);

%%%%%%%%%%%%%%%%%%%%%%%%%%%%%%%%%%%%%%%%
%PART III, give the difference of the x, y, z coordinate difference of        %
%sensor i to sensor 1. The values are stored in Matrix xyzione()              %
%%%%%%%%%%%%%%%%%%%%%%%%%%%%%%%%%%%%%%%%
h = waitbar(0, 'Positioning in progress...');
NumOfSamples = 50;
for ks = 1 : NumOfSamples
    %waitbar(ks/NumOfSamples)
    sensors(1,:)=sensorLocation(1,:);      file1=['nov15/sensor1/sensor1_'      num2str(ks)      '.txt'];
K(1)=Kall(1);
    for ksin = 1 : NumOfSamples
```

```
    sensors(2,:)=sensorLocation(2,:); file2=['nov15/sensor2/sensor2_' num2str(ksin) '.txt']; K(2)=Kall(2);
    sensors(3,:)=sensorLocation(4,:); file3=['nov15/sensor4/sensor4_' num2str(ksin) '.txt']; K(3)=Kall(4);
    sensors(4,:)=sensorLocation(5,:); file4=['nov15/sensor5_1/sensor5_' num2str(ksin) '.txt']; K(4)=Kall(5);

    xyzione=zeros(3,3);
    for m=1:3
      xyzione(m,:)=sensors(m+1,:)-sensors(1,:);
    end
    xyzione;

    %%%%%%%%%%%%%%%%%%%%%%%%%%%%%%%%%%%%%%%%%%%%%%%
    %PART IV, give the distance difference between sensor i to sensor 1 by calling        %
    %function TDOA.                                                                        %
    %%%%%%%%%%%%%%%%%%%%%%%%%%%%%%%%%%%%%%%%%%%%%%%

    %call TDOA to get time delay and distance differences between sensor i to
    %source from convolution/cross correlation or leading edge with FIR filter
    rione=zeros(3,1);
    soundSpeed=1480*1e3;      %mm/sec
    %T=TDOA1(file1,file2,file3,file4);
    T=TDOADSP(file1,file2,file3,file4);

    rioneConv=(T(1:3)*soundSpeed)';
    rione=rioneConv;

    %%%%%%%%%%%%%%%%%%%%%%%%%%%%%%%%%%%%%%%%%%%%
    %PART V, Form the equation and find the distance from sensor1 to the          %
    %acoustic source r1.                                                           %
    %%%%%%%%%%%%%%%%%%%%%%%%%%%%%%%%%%%%%%%%%%%%

    A=-inv(xyzione)*rione;
    for m=1:3
      C(m,1)=(rione(m,1)^2-K(m+1)+K(1))/2;
    end
    B=-inv(xyzione)*C;

    %Give the coefficients of quadrature equation for r1 and find positive solution of r1
    AA=sum(A.^2)-1;
    BB=2*sum(A.*B)-2*sum(sensors(1,:)'.*A);
    CC=sum(sensors(1,:).^2)+sum(B.^2)-2*sum(sensors(1,:)'.*B);

    r1=roots([AA BB CC]);

    %%%%%%%%%%%%%%%%%%%%%%%%%%%%%%%%%%%%%%%%%%%
    %PART V, find x, y, z                                                          %
    %%%%%%%%%%%%%%%%%%%%%%%%%%%%%%%%%%%%%%%%%%%
    xyz1=A*r1(1,1)+B;
    xyz2=A*r1(2,1)+B;
```

```
        indexofxyz = (ks-1)*NumOfSamples+ksin;
        if sum((xyz1'-source).^2) < sum((xyz2'-source).^2)
            xyz(indexofxyz, :)=xyz1';
        else
            xyz(indexofxyz, :)=xyz2';
        end
        fractions = [num2str(indexofxyz/NumOfSamples^2*100) '% is done'] ;
        waitbar(indexofxyz/NumOfSamples^2, h, fractions);%, [fractions]+'% finished')
    end
end

close(h)
figure
stem3(sensors(:,1), sensors(:,2), sensors(:,3))
hold on
stem3(source(1), source(2), source(3))
stem3(xyz(:, 1), xyz(:, 2), xyz(:, 3),'*')

xlabel('x-mm')
ylabel('y-mm')
zlabel('z-mm')
grid on
```

2. Coordinate function

```
function out = coordinate(par, ox, oy, xy)

%system coordinates
x1=ox;
x2=((oy^2-xy^2)/ox+ox)/2;
y2=sqrt(oy^2-x2^2);
%coordinates of sensor/source
O=par(1); X= par(2); Y=par(3);
x=((O^2-X^2)/x1+x1)/2;
y=((O^2-Y^2+(x-x2)^2-x^2)/y2+y2)/2;
z=sqrt(O^2-x^2-y^2);
out=[x y z];
%end of function coordinate
```

3. TDOA1 function for convolution method

```
function [T]=TDOA1(f1, f2, f3, f4)
%%%%%%%%%%%%%%%%%%%%%%%%%%%%%%%%%%%%%%%%%%%%% %
%   This function loads the four waveforms from four different sensors, plots       %
%   the waveforms and mark the maximum point of each waveform.                      %
%   Then convolutions between sensor i to sensor 1 are performed and                %
%   the time delay is returned to the main program. Also the convolution            %
%   between sensor i and sensor1 is plotted out. The maximum point of each          %
%   convolution trace is given                                                      %
%%%%%%%%%%%%%%%%%%%%%%%%%%%%%%%%%%%%%%%%%%%%%%

%load sensor waveforms and plot waveforms
```

```
a1=load(f1);
a2=load(f2);
a3=load(f3);
a4=load(f4);
%sensor1_1(:,1)=a1(1:14000,1);sensor1_1(:,2)=a1(1:14000,2);
sensor1_1(:,1)=a1(1:14000,1);sensor1_1(:,2)=a1(1:14000,2);
sensor2_1(:,1)=a2(1:14000,1);sensor2_1(:,2)=a2(1:14000,2);
sensor3_1(:,1)=a3(1:14000,1);sensor3_1(:,2)=a3(1:14000,2);
sensor4_1(:,1)=a4(1:14000,1);sensor4_1(:,2)=a4(1:14000,2);


delta_t=sensor1_1(2,1)-sensor1_1(1,1);
[lb,mb]=max(abs(sensor2_1(:,2)));
[nb,ob]=max(abs(sensor3_1(:,2)));
[pb,qb]=max(abs(sensor4_1(:,2)));
[ab,bb]=max(abs(sensor1_1(:,2)));
tt=-[bb-mb bb-ob bb-qb]*delta_t;

% subplot(4,1,1)
% plot(sensor1_1(:,1),sensor1_1(:,2),'r')
% ylabel('amplitude')
% hold on
% plot(sensor1_1(bb,1),ab,'*')
% title('Signal from sensor1')
% subplot(4,1,2)
% plot(sensor2_1(:,1),sensor2_1(:,2),'g')
% hold on
% plot(sensor2_1(mb,1),lb,'*')
% title('Signal from sensor2')
% subplot(4,1,3)
% plot(sensor3_1(:,1),sensor3_1(:,2),'b')
% hold on
% plot(sensor3_1(ob,1),nb,'*')
% title('Signal from sensor3')
% subplot(4,1,4)
% plot(sensor4_1(:,1),sensor4_1(:,2),'k')
% hold on
% plot(sensor4_1(qb,1),pb,'*')
% title('Signal from sensor4')
% xlabel('time-sec')

%Convolve the signals from sensor i to sensor1 and find time delay

h1=conv(sensor1_1(:,2),sensor2_1(:,2));
h2=conv(sensor1_1(:,2),sensor3_1(:,2));
h3=conv(sensor1_1(:,2),sensor4_1(:,2));
g1=conv(sensor1_1(:,2),sensor1_1(:,2));

[l,m]=max(abs(h1));
[n,o]=max(abs(h2));
[p,q]=max(abs(h3));
```

```
[a,b]=max(abs(g1));

delta_t=sensor1_1(2,1)-sensor1_1(1,1);
t21=(m-b).*delta_t;
t31=(o-b).*delta_t;
t41=(q-b).*delta_t;

T=[t21 t31 t41 tt(1) tt(2) tt(3)];

% figure
% subplot(4,1,1)
% plot((1:size(abs(h1)))*delta_t, real(h1), 'r')
% hold on
% plot(m*delta_t,l,'*')
% title('convolution of signals between sensor1 and sensor2')
% subplot(4,1,2)
% plot((1:size(abs(h2)))*delta_t, real(h2), 'g')
% hold on
% plot(o*delta_t,n,'*')
% title('convolution of signals between sensor1 and sensor2')
% subplot(4,1,3)
% plot((1:size(abs(h3)))*delta_t, real(h3), 'b')
% hold on
% plot(q*delta_t,p,'*')
% title('convolution of signals between sensor1 and sensor2')
% subplot(4,1,4)
% plot((1:size(abs(g1)))*delta_t, real(g1), 'k')
% hold on
% plot(b*delta_t,a,'*')
% title('convolution of signals from sensor1')
```

4. TDOA1 function for cross-correlation method

```
function [T]=TDOA1(f1, f2, f3, f4)

a1=load(f1);
a2=load(f2);
a3=load(f3);
a4=load(f4);
sensor1_1(:,1)=a1(1:14000,1);sensor1_1(:,2)=a1(1:14000,2);
sensor2_1(:,1)=a2(1:14000,1);sensor2_1(:,2)=a2(1:14000,2);
sensor3_1(:,1)=a3(1:14000,1);sensor3_1(:,2)=a3(1:14000,2);
sensor4_1(:,1)=a4(1:14000,1);sensor4_1(:,2)=a4(1:14000,2);
delta_t=sensor1_1(2,1)-sensor1_1(1,1);
[lb,mb]=max(abs(sensor2_1(:,2)));
[nb,ob]=max(abs(sensor3_1(:,2)));
[pb,qb]=max(abs(sensor4_1(:,2)));
[ab,bb]=max(abs(sensor1_1(:,2)));
tt=-[bb-mb bb-ob bb-qb]*delta_t;
```

```
h1=xcorr(sensor1_1(:,2),sensor2_1(:,2));
h2=xcorr(sensor1_1(:,2),sensor3_1(:,2));
h3=xcorr(sensor1_1(:,2),sensor4_1(:,2));
g1=xcorr(sensor1_1(:,2),sensor1_1(:,2));

[l,m]=max(abs(h1));
[n,o]=max(abs(h2));
[p,q]=max(abs(h3));
[a,b]=max(abs(g1));

delta_t=sensor1_1(2,1)-sensor1_1(1,1);
t21=(m-b).*delta_t;
t31=(o-b).*delta_t;
t41=(q-b).*delta_t;

T=[t21 t31 t41 tt(1) tt(2) tt(3)];
```

5. TDOADSP for leading edge method

```
function [T]=TDOADSP(f1, f2, f3, f4)
%load sensor waveforms and plot waveforms
a1=load(f1);
a2=load(f2);
a3=load(f3);
a4=load(f4);
sensor1_1(:,1)=a1(1:14000,1);sensor1_1(:,2)=a1(1:14000,2);
sensor2_1(:,1)=a2(1:14000,1);sensor2_1(:,2)=a2(1:14000,2);
sensor3_1(:,1)=a3(1:14000,1);sensor3_1(:,2)=a3(1:14000,2);
sensor4_1(:,1)=a4(1:14000,1);sensor4_1(:,2)=a4(1:14000,2);

load PDfilter3
%freqz(Num,[1],4096)
sensor1_1(:,2) = filter(Num, 1 ,sensor1_1(:,2));
sensor2_1(:,2) = filter(Num, 1 ,sensor2_1(:,2));
sensor3_1(:,2) = filter(Num, 1 ,sensor3_1(:,2));
sensor4_1(:,2) = filter(Num, 1 ,sensor4_1(:,2));

delta_t=sensor1_1(2,1)-sensor1_1(1,1);
[lb,mb]=max(abs(sensor2_1(:,2)));
[nb,ob]=max(abs(sensor3_1(:,2)));
[pb,qb]=max(abs(sensor4_1(:,2)));
[ab,bb]=max(abs(sensor1_1(:,2)));
tt=-[bb-mb bb-ob bb-qb]*delta_t;
T=tt;
```